REFERENCES

Ajili, S.H., Ebrahimi, N.G., and Soleimani, M. (2009) Polyurethane/polycaprolactane blend with shape memory effect as a proposed material for cardiovascular implants. Acta Biomaterialia, 5, 1519–1530.

Almquist, R. (2010) Electrochemical synthesis of electroactive polymers for drug release for bio scaffolds. M.S. Thesis, Karolinska Institutet, Department of Cell and Molecular Biology, Solna, Sweden.

Bar-cohen, Y. (2002), Artificial Muscles using Electroactive Polymers (EAP); Current capabilities and challenges. Paper presented at the SPIE Smart Structures and Materials Symposium, EAPAD Conference, San Diego, CA, USA.

Bonagamba, T.J., Bello, Jr. B., Giotto, M.V., Panepucci, H., Magon, C.J., and Campos, M.S. (1995) Iron doping effects on the high-resolution 13CNMR spectra of solid poly(para-phenylene). Synthetic Metals, 68, 103-108.

Bouzakraoui, S., Bouzzine, S.M., Bouachrine, M., and Hamidi, M. (2005) Density functional theory study of conformational and opto-electronic properties of oligo-para-phenylenes. Theochem, 725, 39–44.

Brown, P.J., Gandy, A.P., Ishida, K., Kainuma, R., Kanomata, T., Matsumoto, M., Morito, H., Neumann, K.-U., Oikawa, K., Ouladdiaf, B., and Ziebeck, K.R.A. (2007) Magnetic shape memory behaviour. Journal of Magnetism and Magnetic Materials, 310, 2755-2760.

Brédas, J.L., Thémas, B., and André, J.M. (1982) Electronic structure of highly conducting poly-(p-phenylene) chains: An ab initio Hartree-Fock Study. Physical Review B, 26, 6000-6002.

Chang, Y.W., Eom, J.P., Kim, J.G., Kim, H.T., and Kim, D.K. (2010) Preparation and characterization of shape memory polymer networks based on carboxylatedtelechelic poly(ε-caprolactone)/epoxidized natural rubber blends. Journal of Industrial and Engineering Chemistry, 16, 256-260.

Choi, M.C., Kim, Y., and Ha, C.S. (2008) Polymers for flexible displays: From material selection to device applications. Progress in Polymer Science, 33, 581-630.

Colwell, J.M. (2006) Synthesis of Polycaprolactone Polymers for Bone Tissue Repair. A thesis submitted for the degree of Doctor of Philosophy, School of Physical and Chemical Sciences, Queensland University of Technology.

Darwis, D., Mitomo, H., Enjoji, T., Yoshii, F., and Makuuchi, K. (1998) Enzymatic degradation of radiation crosslinkedpoly(ε-caprolactone). Polymer Degradation and Stability, 62, 259-265.

Fabrizio, Q.,Loredana, S., and Anna, S.E. (2012) Shape memory epoxy foams for space applications. Materials Letters, 69, 20-23.

Golovtsov, I. (2005) Modification of conductive properties and processability of polyparaphenylene, polypyrrole and polyaniline. Ph.D. dissertation. Tallinn University of Technology.

Guimard, N.K., Gomez, N., and Schmidt, C.E. (2007) Conducting polymers in biomedical engineering. Progress in Polymer Science, 32, 876-921.

Gunes, I.S., Jimenez, G.A., and Jana, S.C. (2009) Carbonaceous fillers for shape memory actuation of polyurethane composites by resistive heating. Carbon, 47, 981–997.

Han, C., Ran, X., Su, X., Zhang, K., Liu, N., and Dong L. (2007) Effect of peroxide crosslinking on thermal and mechanical properties of poly(ε-caprolactone), Polymer International, 56, 593-600.

Harun, M.H., Saion, E., Kassim, A., Yahya, N. and Mahmud, E. (2007) Conjugated Conducting Polymers: A Brief Overview. JASA, 2, 63-68

Hérold, C. and Billaud, D. (1990) Electrochemical doping of polyparaphenylene with alkali metals in solid state cell. Solid State Ionics, 40/41, 985-987.

Hiumtup, P., Sirivat, A., and Jamieson A.M. (2008) Electromechanical response of a soft and flexible actuator based on polyaniline particles embedded in a cross-linked poly(dimethyl siloxane) network. Materials Science and Engineering C, 28, 1044-1051.

Huang, W.M., Ding, Z., Wang, C.C., Wei, J., Zhao, Y., and Purnawali, H. (2002) Shape memory materials. Materials Today, 13, 54-61.

Jung, Y.C., Yoo, H.J., Kim, Y.A., Cho, J.W., and Endo, M. (2010) Electroactive shape memory performance of polyurethane composite having homogeneously dispersed and covalently crosslinked carbon nanotubes. Carbon, 48, 1598–1603.

Kaynak, A. (1997) DC conduction in electrochemically synthesized polypyrrole films. Turkish Journal of Chemistry, 22, 81-85.

Kim, K.J. and Tadokoro, S. (2007) Electroactive Polymers for Robotic Application: artificial muscles and sensors. London: Springer-Verlag.

Koo, C.M. (2012) Electroactive Thermoplastic dielectric elastomers as a new generation polymer actuators. Thermoplastic Elastomer, 400-416.

Kunanuruksapong, R. and Sirivat, A. (2007) Poly(p-phenylene) and acrylic elastomer blends for electroactive application. Materials Science and Engineering A, 454–455, 453–460.

Kunchornsup, W. And Sirivat, A. (2012) Physically cross-linked cellulosic gel via 1-butyl-3-methylimidazolium chloride ionic liqiud and its electromechanical response. Sensors and Actuators A, 175, 155-164.

Lee, K.M., Knight, P.T., Chung, T., And Mather, P.T. (2008) Polycaprolactone-POSS Chemical/Physical Double Networks.Macromolecules, 41, 4730-4738.

Li, S., Li, Z., Fang, X., Chen, G.Q., Huang, Y. and Xu, K. (2008) Synthesis and characterization of polyparaphenylene from cis-dihydrocatechol. Journal of Applied Polymer Science, 110, 2085–2093.

Liu,Y., Lv, H., Lan, X., Leng, J., and Du, S. (2009) Review of electro-active shape-memory polymer composite. Composites Science and Technology, 69, 2064–2068.

MacDiarmid, A.C. (2001) "Synthetic Metals": A Novel Role for Organic Polymers (Novel Lecture). Angewante Chemie, 40, 2581-2590.

Majoumo-Mbe, F., Smolensky, E., Lönnecke, P., Shpasser D.D., Eisen, M.S., and Hey-Hawkins, E. (2005) Polymerisations of ε-caprolactone and β-butyrolactone with Zn-, Al- and Mg-based organometallic complexes. Journal of Molecular Catalysis A: Chemical, 240, 91-98.

Meng, Q. and Hu, J. (2009) A review of shape memory polymer composites and blends. Composites: Part A, 40, 1661–167.2

Mo-Ling, C. (1999) *Polymers as low-temperature thermoplastic splinting material*, M.S. Thesis, The Hong Kong Polytechnic University, Hong Kong.

Olaru, P., Hutchings, I., and Dorr, N (2010) Shape memory polymers-(SMPs) nanostrip multilayers applied on the new bearing generation for hard wearing in turbocharges. Paper presented at The 17th International Colloquium of Tribology, 19-21.

Pandini, S., Passera, S., Messori, M., Paderni, K., Toselli, M., Gianoncelli, A., Bontempi, E., and Riccò, T. (2012) Two-way reversible shape memory behaviour of crosslinked poly(ε-caprolactone). Polymer, 1-10.

Park, J.M., Lee, S.I., and Choi, J.H. (2005) Cure monitoring and residual stress sensing of single-carbon fiber reinforced epoxy composites using electrical resistivity measurement. Composite Science and Technology, 65, 571-580.

Petit, L., Guiffard, B., Seveyrat, L., and Guyoma,r D. (2008) Actuating abilities of electroactive carbon nanopowder/polyurethane composite films. Sensors and Actuators A: Physical, 148, 105-110.

Phumman, P., Niamlang, S., and Sirivat, A. (2009) Fabrication of poly(p-phenylene)/zeolite composites and their responses towards ammonia. Sensors, 9, 8031-8046.

Ping, P., Wang, W., Chen, X., and Jing, X. (2005) Poly(ε-caprolactone) Polyurethane and Its Shape-Memory Property. Biomacromolecules, 6, 587-592.

Plocharski, J. and Wycislik, H. (2000) Mixed conductivity in poly(p-phenylene) doped with iron chloride. Solid State Ionics, 127, 337–344.

Pratt, C. (1996) Conducting Polymers. Retrieved April 16 2012 from http://homepage.ntlworld.com/colin.pratt/cpoly.pdf.

Puvanatvattana, T., Chotpattananont, D., Hiumtup, P., Niamlang, S., Sirivat, A. and Jamieson A.M. (2006) Electric field induced stress moduli in polythiophene/polyisoprene elastomer blends. Reactive & Functional Polymers, 66, 1575-1588.

Rabani, G.,Luftmann, H., and Kraft, A. (2006) Synthesis and characterization of two shape-memory polymers containing short aramid hard segments and poly(ε-caprolactone) soft segments. Polymer, 47, 4251-4260.

Runge, M.B., Dadsetan, M., Baltrusaitis, J., Knight, A.M., Ruesink, T., Lazcano, E.A., Lu, L., Windebank, A.J., and Yaszemski, M.J. (2010) The development of electrically conductive polycaprolactone-polypyrrole composite materials for nerve regeneration. Biomaterials, 31, 5916-5926.

Sahoo, N.G., Jung Y.C., Yoo, H.J., and Cho, J.W. (2007) Influence of carbon nanotubes and polypyrrole on the thermal, mechanical and electroactive shape memory properties of polyurethane nanocomposites. Composite Science and Technology, 67, 1920-1929.

Samatham, R., Kim, K.J., Dogruer, D., Choi, H.R., Konyo, M., Madden, J.D., Nakabo, Y., Nam, J.D., Su, J., Tadokoro, S., Yim, W., and Yamakita, M. (2007). Electroactive Polymers for Robotic Application; artificial muscles and sensors, London: Springer-Verlag.

Small IV, W., Singhal, P., Wilson, T.S., and Maitland, D.J. (2009) Biomedical applications of thermally activated shape memory polymers. Journal of Materials Chemistry, Lawrence Livermore National Laboratory, USA.

Snyder, A.J., Tews, A.M., Frecker M.I., Zhang, G., and Runt J.P. (2003) Biomedical Applications of Electroactive Polymers. Paper presented at The 5th International Conference on Intelligent Materials, Pennsylvania, USA

Sodhi, J.S., and Rao, I.J. (2010) Modeling the mechanics of light activated shape memory polymers. International Journal of Engineering Science, 48, 1576-1589.

Sohn, J.I., Sung J.H., Choi, H.J., and Jhon, M.S. (2002) The Effect of Particle Concentration of Poly(p-phenylene) on Electrorheological Response. Journal of Applied Polymer Sciences, 84, 2397-2403.

Vinogradov, A., Su, J., Jenkins, C., and Bar-cohen Y. (2006) *State-of-the-Art Developments in the Field of Electroactive Polymers*, MRS Proceedings, Vol. 889.

Wei, Z.G. and Sandstörm, R. (1998) Review Shape-memory materials and hybrid composites for smart systems. Journal of Materials Science, 33, 3743-3762.

Woodruff, M.A. and Hutmacher, D.W. (2010) The return of a forgotten polymer - Polycaprolactone in the 21st century. Progress in Polymer Science, 35, 1217-1256.

Xiao, Y., Zhou, S., Wang, L., and Gong, T. (2010) Electro-active Shape Memory Properties of Poly(ε-caprolactone)/Functionalized Multiwalled Carbon Nanotube Nanocomposite. Applied materials and interfaces, 2, 3506-3514.

Yuan, P. (2010) Biodegradable Shape-Memory Polymers. Literature Seminar

Zhang, H. , Wang, H., Zhong, W., and Du, Q. (2009) A novel type of shape memory polymer blend and the shape memory mechanism. Polymer, 50, 1596-1601.

Zhu, G., Xu, Q., Qin, R., Yan, H., and Liang, G. (2005) Effect of γ-radiation on crystallization of polycaprolactone. Radiation Physics and Chemistry, 74, 42-50.

Appendices

Appendix A Fingerprint Peaks of FT-IR Spectra of Poly(p-phenylene) (PPP)

Functional groups of undoped and doped poly(p-phenylene) were characterized by using the FT-IR spectrophotometer (Nicolet, Nexus 670). The experiment was operated in the transmission mode in the wavenumber range of 400-4000 cm^{-1} with 64 scans and $\pm$ 4 cm^{-1}. The sample was dried before grinding and then mixed with dried potassium bromide (KBr) which was used as a background material.
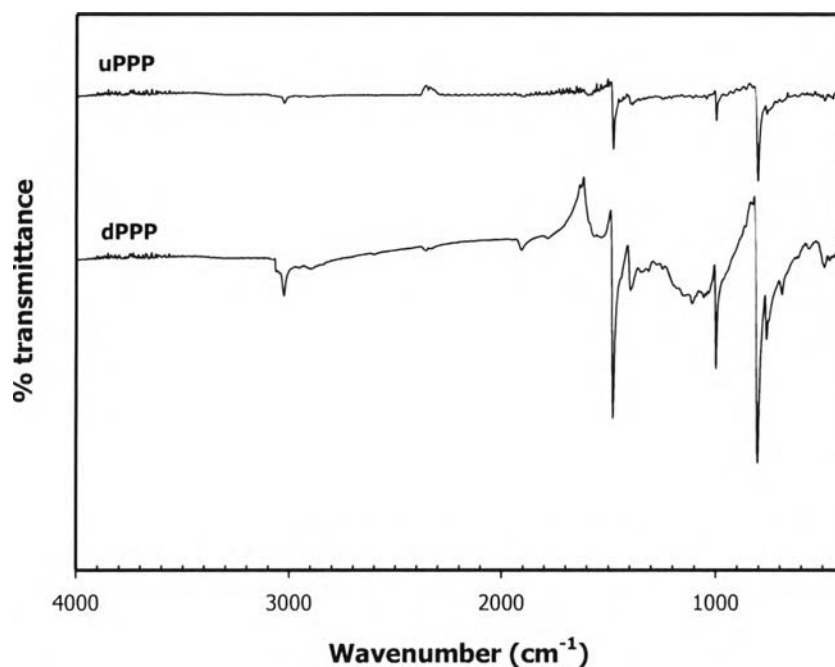
Figure A1 FT-IR spectra of uPPP and dPPP.

The FT-IR spectra of synthesized PPP via the oxidative cationic polymerization (Plocharski *et al.*, 2000) show transmission peaks at 692,764 and 805 cm^{-1} which can be assigned to the C-H out of plane vibration of the mono

substituted benzene ring (Sohn *et al.*, 2001). The highly intense peak at 999 cm⁻¹ can be assigned to the C-C stretching of the benzene ring (Kunanuraksapong *et al.*, 2009). Furthermore, other intense peaks at 1392 and 1479 cm⁻¹ can be assigned to the para-disubstitution of the benzene ring (Phumman *et al.*, 2007).

Using iron(III) chloride as the dopant causes an additional transmission peaks in the spectra. The peaks appear at 1110 and 1559 cm⁻¹ which can be attributed to the intrinsic vibration in the doping state of the polymer which does not appear in the undoped state (Phumman *et al.*, 2007).

Table A1 Peak assignments of PPP

Wavenumber (cm-1)	Assignment	References
692	C-H out of plane vibration of mono substituted benzene ring	Dubois *et al.*, 2001
764	C-H out of plane vibration of mono substituted benzene ring	Dubois *et al.*, 2001
805	C-H out of plane vibration of mono substituted benzene ring	Sohn *et al.*, 2001
999	C-C Stretching of benzene ring	Kunanuraksapong *et al.*, 2009
1392	C-H out of plane vibration of para disubstituted benzene ring	Phumman *et al.*, 2007
1479	C-H out of plane vibration of para disubstituted benzene ring	Sohn *et al.*, 2001
3026	C-H stretching of benzene ring	Li *et al.*, 2008

Appendix B Thermal Property

Thermal properties of uPPP and 30:1 dPPP were investigated by using the thermogravimetricanalyser (Perkin Elmer, TGA7). The experiment was operated from 30-900°C with the heating rate of 10°C/min and under nitrogen atmosphere. The sample was weighted in the range of 5-20mg before loaded into a platinum pan. The thermogram from figure B1 shows that both uPPP and 30:1 dPPP do not decompose visibly below 600 °C, they begin to decompose at approximately 700°C but not completely even at temperature up to 900°C that can be concluded that both of uPPP and dPPP have good thermal stability.

Thermogram of dPPP suggests a higher rate of degradation than the undoped one. This means that dPPP has less thermal stability when temperature increases because of the defect of counterions in the PPP backbone.
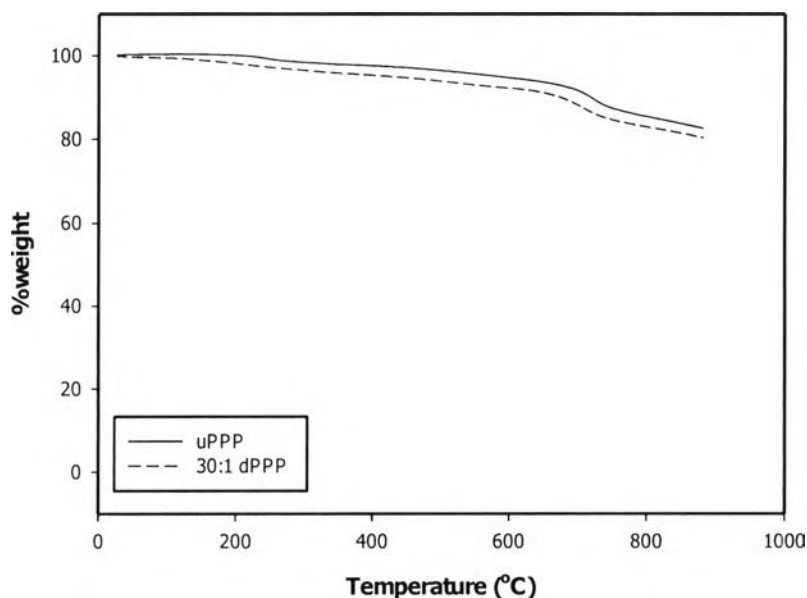
Figure B1 TGAthermogram of uPPP and 30:1 dPPP.

For PCL and crosslinked PCL matrix, there is dramatically weight loss at approximately 384 and 368°C, respectively, which can be contributed to the PCL chain decomposition. For the PCL/PPP composite, the decomposition temperature is

approximately 370°C. Furthermore, the weight remains after the experiment increase when increase the concentration of embedded PPP which is not degrade completely although the temperature rises to 900°C.
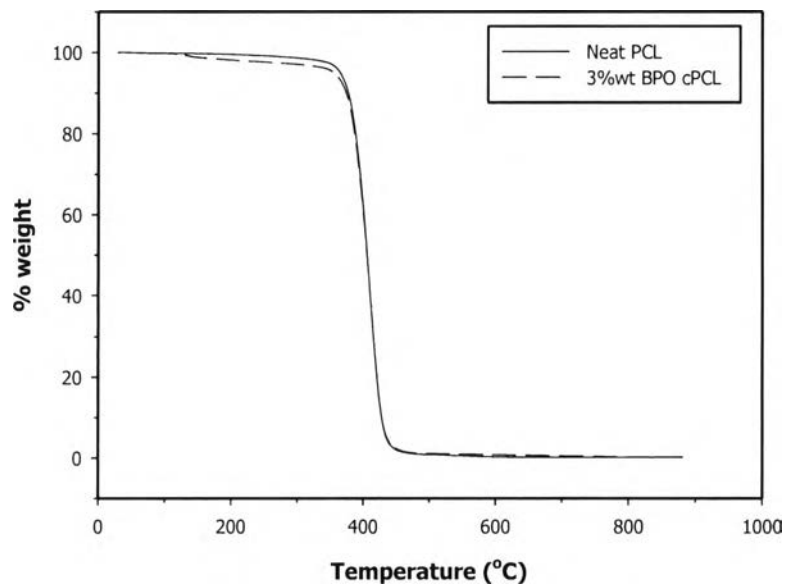
Figure B2 TGAthermogram ofPCL and 3%wt BPO cPCL.
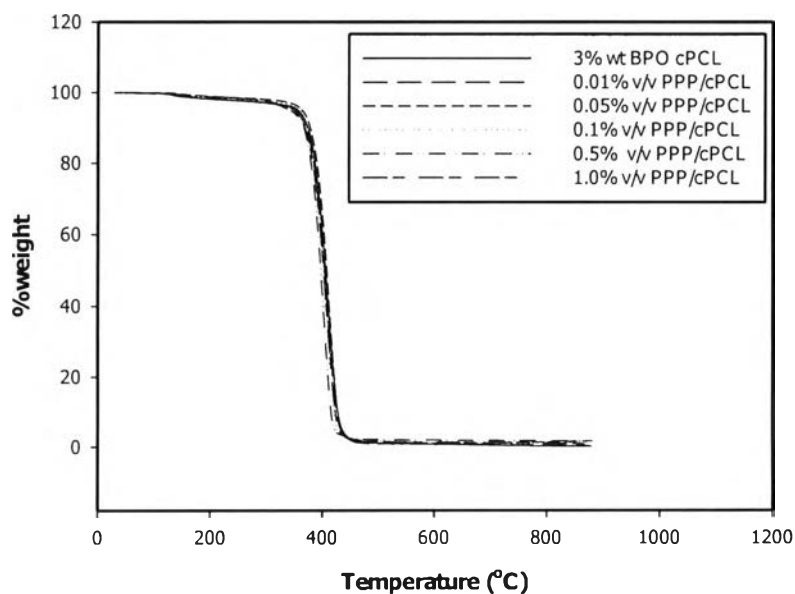
Figure B3 TGAthermogram of cPCL and its composite.

Table B1 Decomposition temperature, initial and final wight of uPPP and 30:1 dPPP

Sample	T_d ($^{\circ}$C)	Initial wight (mg)	Final weight (mg)
uPPP		7.22	6.03
30:1 dPPP		5.79	4.78

Table B2 Decomposition temperature, initial and final wight of cPCL and its composite at various concentration of PPP

Sample	T_d ($^{\circ}$C)	Initial wight (mg)	Final weight (mg)
PCL	384.18	15.04	0.032
3%wt BPO cPCL	368.72	15.03	0.025
0.01%v/v PPP/cPCL	367.41	15.89	0.049
0.05%v/v PPP/cPCL	369.15	16.38	0.056
0.1%v/v PPP/cPCL	369.08	15.35	0.066
0.5%v/v PPP/cPCL	370.46	15.87	0.071
1.0%v/v PPP/cPCL	367.68	15.53	0.118

Appendix C Density Measurement of Poly(p-phenylene) (PPP)

The density of uPPP was measured out by using a gas pycnometer (Quantachrome Instrument, Ultrapycnometer 1000). The operation was repeated for 20 times under ultra high purity helium atmosphere with the purge time of 1 minute.

Table C1 Comparison of the density of the PPP particle

Run number	Average density (g/cm^3)	Standard deviation
uPPP	1.366	0.037
1:30 dPPP	1.466	0.027
30:1 dPPP	1.634	0.008
100:1 dPPP	1.846	0.036

Table C2 Raw data of density of uPPP

Run number	Volume (cm^3)	Density (cm^3)
1	0.407	1.397
2	0.419	1.358
3	0.423	1.345
4	0.400	1.422
5	0.428	1.329
6	0.409	1.391
7	0.414	1.374
8	0.407	1.398
9	0.416	1.367
10	0.417	1.366

Run number	Volume (cm^3)	Density (cm^3)
11	0.430	1.323
12	0.438	1.299
13	0.417	1.366
14	0.409	1.391
15	0.415	1.372
16	0.411	1.384
17	0.396	1.436
18	0.414	1.376
19	0.428	1.331
20	0.410	1.387

Table C2 Raw data of density of 1:30 dPPP

Run number	Volume (cm^3)	Density (cm^3)
1	0.358	1.593
2	0.376	1.513
3	0.403	1.414
4	0.387	1.471
5	0.395	1.441
6	0.389	1.462
7	0.371	1.534
8	0.378	1.505
9	0.376	1.515
10	0.389	1.463

Run number	Volume (cm^3)	Density (cm^3)
11	0.387	1.469
12	0.392	1.452
13	0.378	1.505
14	0.385	1.478
15	0.396	1.439
16	0.394	1.446
17	0.377	1.509
18	0.384	1.483
19	0.401	1.419
20	0.389	1.465

Table C3 Raw data of density of 30:1 dPPP

Run number	Volume (cm^3)	Density (cm^3)
1	0.734	1.647
2	0.729	1.664
3	0.745	1.629
4	0.735	1.649
5	0.726	1.671
6	0.726	1.672
7	0.734	1.654
8	0.737	1.646
9	0.743	1.632
10	0.744	1.631

Run number	Volume (cm^3)	Density (cm^3)
11	0.749	1.619
12	0.743	1.631
13	0.741	1.638
14	0.742	1.635
15	0.748	1.623
16	0.737	1.647
17	0.742	1.636
18	0.740	1.639
19	0.739	1.641
20	0.742	1.636

Table C4 Raw data of density of 100:1 dPPP

Run number	Volume (cm^3)	Density (cm^3)
1	0.465	1.845
2	0.465	1.847
3	0.469	1.831
4	0.449	1.911
5	0.466	1.842
6	0.475	1.807
7	0.468	1.835
8	0.473	1.812
9	0.464	1.852
10	0.454	1.892

Run number	Volume (cm^3)	Density (cm^3)
11	0.459	1.872
12	0.444	1.934
13	0.471	1.823
14	0.469	1.830
15	0.457	1.877
16	0.473	1.816
17	0.471	1.821
18	0.465	1.847
19	0.472	1.818
20	0.471	1.823

Appendix D Particle Size and Particle Size Distribution of Poly(p-phenylene) (PPP)

A particle size analyser (Malvern, Mastersizer X) was used to determine the particle size and the particle size distribution of uPPP. uPPP was ground in the mortar by pestle before the examination.

Table D1 Average particle size of uPPP

Sample	Average particle diameter (μm)				
	1	2	3	average	SD
PPP	91.2	91.6	91.8	91.5	0.309

Table D2 Raw data of particle size of PPP

particle size diameter (μm)		uPPP					
		1		2		3	
Size low	Size high	ln%	under%	ln%	under%	ln%	under%
0.50	1.32	0.13	0.13	0.14	0.14	0.15	0.15
1.32	1.60	0.38	0.51	0.41	0.55	0.43	0.58
1.60	1.95	0.53	1.05	0.57	1.11	0.60	1.18
1.95	2.38	0.56	1.61	0.60	1.71	0.63	1.82
2.38	2.90	0.51	2.12	0.54	2.25	0.56	2.38
2.90	3.53	0.44	2.56	0.46	2.70	0.48	2.86
3.53	4.30	0.41	2.97	0.42	3.12	0.44	3.30
4.30	5.24	0.47	3.45	0.48	3.61	0.50	3.80
5.24	6.39	0.68	4.12	0.70	4.31	0.73	4.53
6.39	7.78	1.09	5.22	1.14	5.45	1.19	5.72
7.78	9.48	1.82	7.04	1.89	7.34	1.97	7.69
9.48	11.55	3.04	10.08	3.14	10.48	3.26	10.94

particle size diameter (µm)		uPPP					
		1		2		3	
Size low	Size high	In%	under%	In%	under%	In%	under%
11.55	14.08	4.89	14.98	5.03	15.52	5.18	16.13
14.08	17.15	7.23	22.21	7.38	22.90	7.56	23.68
17.15	20.90	9.45	31.65	9.59	32.49	9.74	33.42
20.90	25.46	10.52	42.17	10.61	43.09	10.66	44.08
25.46	31.01	10.13	52.29	10.10	53.20	10.03	54.10
31.01	37.79	8.79	61.09	8.64	61.84	8.45	62.55
37.79	46.03	6.98	68.06	6.74	68.58	6.48	69.03
46.03	56.09	4.90	72.96	4.64	73.22	4.39	73.42
56.09	68.33	2.79	75.75	2.58	75.80	2.39	75.82
68.33	83.26	0.98	76.72	0.86	76.65	0.76	76.57
83.26	101.44	0.00	76.73	0.00	76.67	0.00	76.59
101.44	123.59	0.00	76.73	0.00	76.67	0.00	76.59
123.59	150.57	0.00	76.73	0.00	76.67	0.00	76.59
150.57	183.44	0.44	77.17	0.38	77.04	0.37	76.96
183.44	223.51	2.49	79.67	2.37	79.42	2.33	79.30
223.51	272.31	5.22	84.89	5.10	84.52	5.03	84.33
272.31	331.77	7.17	92.05	7.20	91.71	7.16	91.48
331.77	404.21	6.02	98.05	6.24	97.93	6.29	97.75
404.21	492.47	1.93	99.98	2.05	99.97	2.23	99.97
492.47	600.00	0.00	100.00	0.00	100.00	0.00	100.00

Appendix E Conductivity Measurement

Electrical conductivity (σ) was measured by a two-point probe connected with a voltage supplier (Keithley, 6517A). The polymers were compressed into pellets at 10 tons with 1 cm diameter. A constant voltage was applied under air atmosphere, 40-60% RH and at 25-27°C, and the current was simultaneously measured then converted into electrical conductivity. The electrical conductivity was calculated from the equation E1:

$$\sigma = 1/\rho = 1/R_s t = I/KVt \qquad \text{(E1)}$$

where σ is the electrical conductivity (S/cm), ρ is the specific resistivity (Ω.cm), R_s is sheet resistance (Ω/sq), I is the measured current (A), V is the applied voltage (V), t is the sample thickness, and K is the geometric correction factor of the two-point probe which can be determined by calibrating the probe with a silicon wafer possessing a known resistivity value.

Table E1 The electrical conductivity of uPPP and each doping level of dPPP

Doping Level	Conductivity (S/cm)	Standard deviation
uPPP	8.14×10^{-6}	8.73×10^{-7}
1:50 dPPP	4.53×10^{-6}	1.66×10^{-6}
1:30 dPPP	1.35×10^{-5}	2.40×10^{-7}
1:1 dPPP	7.85×10^{-5}	4.53×10^{-6}
30:1 dPPP	6.63×10^{-3}	1.43×10^{-4}
50:1 dPPP	9.12×10^{-3}	1.26×10^{-3}
100:1 dPPP	1.48×10^{-2}	8.42×10^{-3}
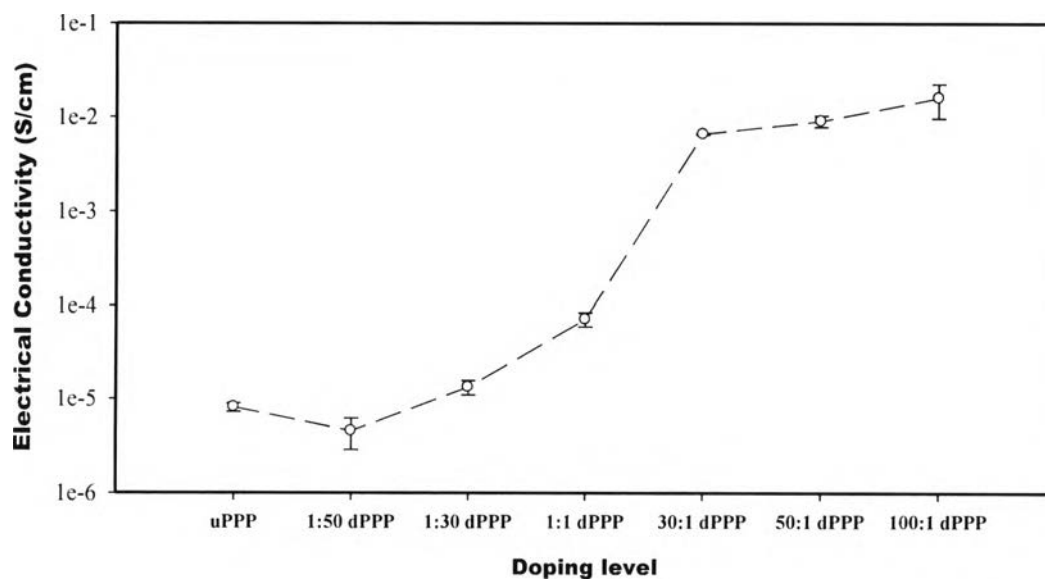
Figure E1 Electrical conductivity of uPPP and dPPP at various doping level.

Table E2 The electrical conductivity of PCL, cPCL film and PCL/PPP composites

Sample	Conductivity (S/cm)	Standard deviation
Neat PCL	3.31×10^{-8}	1.25×10^{-8}
3%wt BPO cPCL	3.63×10^{-8}	6.96×10^{-9}
0.01% v/v PPP/3%wt BPO cPCL	3.32×10^{-8}	1.42×10^{-9}
0.05% v/v PPP/3%wt BPO cPCL	4.39×10^{-8}	1.32×10^{-9}
0.1% v/v PPP/3%wt BPO cPCL	8.39×10^{-8}	8.11×10^{-9}
0.5% v/v PPP/3%wt BPO cPCL	1.01×10^{-7}	6.08×10^{-9}
1% v/v PPP/3%wt BPO cPCL	7.10×10^{-7}	2.54×10^{-7}
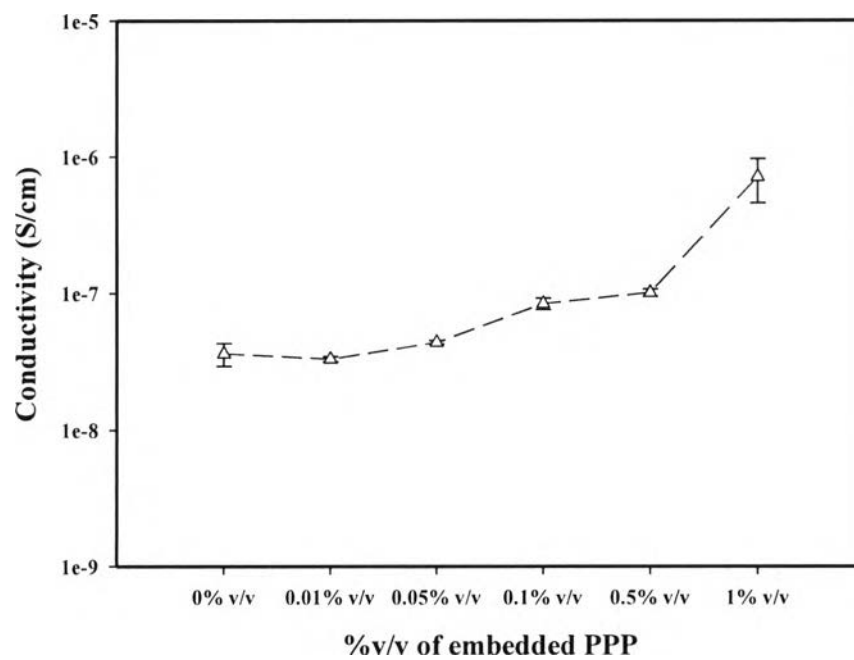
Figure E2 Electrical conductivity of neat cPCL and PPP/cPCL composite at the various concentration.

Appendix F Determination of the Dopant Concentration of Doped PPP

During the doping process, some molecules of the dopant interacted with PPP chain via the electron acceptor to produce polarons and solitons and to increase electrical conductivity (Bonagamda et al.. 1995). To investigate the amount of interacting dopant, iron(III) chloride ($FeCl_3$), the X-ray fluorescence spectrophotometer (PANalytical, Axios PW 4400) was deployed. dPPP was first dried at 100°C for 24 hours then weighted in the range of 0.1-0.2 g and pelletized with 5 g of dried boric acid in an aluminium pan. The operation was done at approximately 25°C and 40-60% RH. Amount of Fe in PPP particle was measured as kilocount per second (kcps) and %concentration.

TableF1 Kcps of Fe in PPP

Doping Level (mole ratio of Fe:PPP monomer)	Kilocount per second (kcps)			Average kcps	Standard deviation
	1	2	3		
1:50 dPPP	0.998	1.267	1.167	1.144	0.135
1:30 dPPP	1.306	0.980	1.226	1.171	0.169
1:1 dPPP	5.481	4.704	4.733	4.973	0.440
30:1 dPPP	51.624	57.084	59.556	56.088	4.058
50:1 dPPP	53.819	59.248	57.471	56.846	2.768
100:1 dPPP	386.995	387.983	385.686	385.686	3.162

TableF2%concentration of Fe in PPP

Doping Level (mole ratio of Fe:PPP monomer)	% concentration of Fe			Average % concentra-tion of Fe	Standard deviation
	1	2	3		
1:50 dPPP	3.92	4.73	4.39	4.35	0.41
1:30 dPPP	6.63	5.01	6.70	6.12	0.96
1:1 dPPP	14.45	11.94	12.23	12.88	1.37
30:1 dPPP	40.99	40.64	39.29	40.30	0.89
50:1 dPPP	44.89	48.37	46.34	46.53	1.74
100:1 dPPP	72.76	72.96	72.94	72.89	0.11
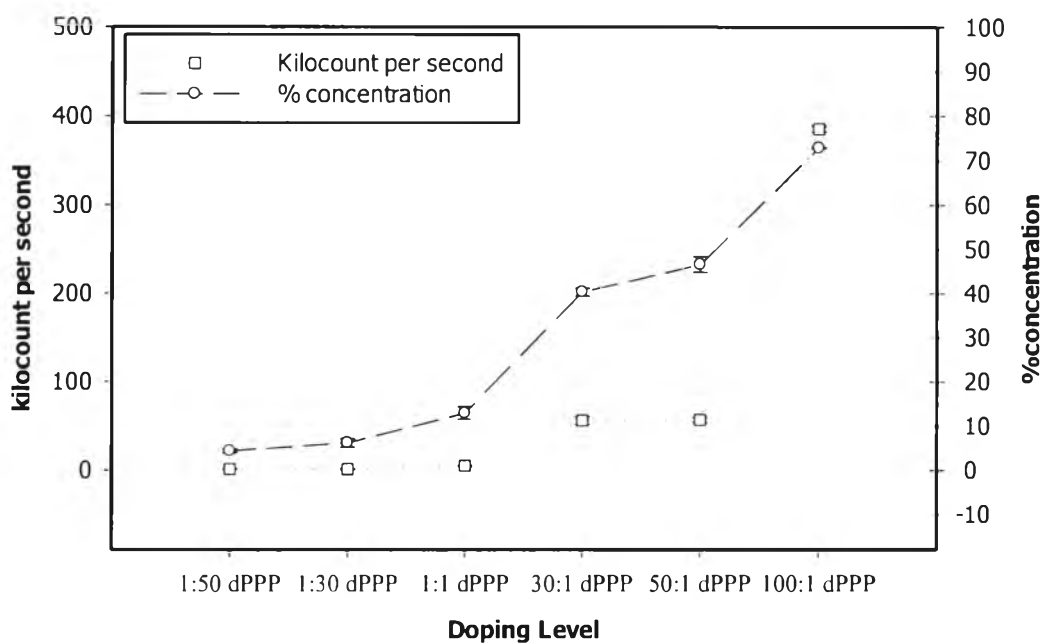
Figure F1 Kcps and %concentration of Fe for each doping level of dPPP.

Appendix G Morphology

The scanning electron microscope (SEM) (Hitachi, S4800) was employed to determine the morphology of PPP, PCL and PPP/PCL composite. First, for PPP particles. The SEM images show that PPP has irregular rod-like shapes.
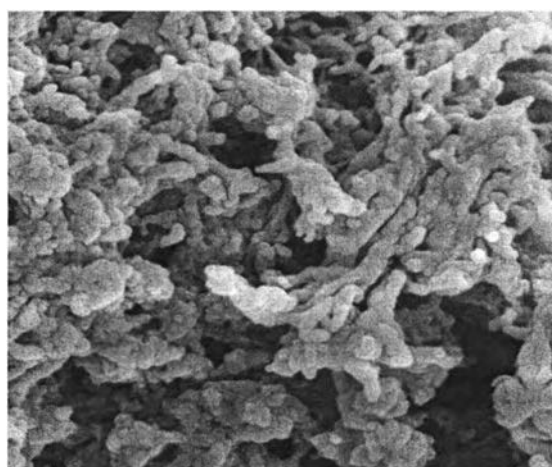
Figure G1 Morphology of uPPPpatricle (15 kV, magnification of 20 kX).
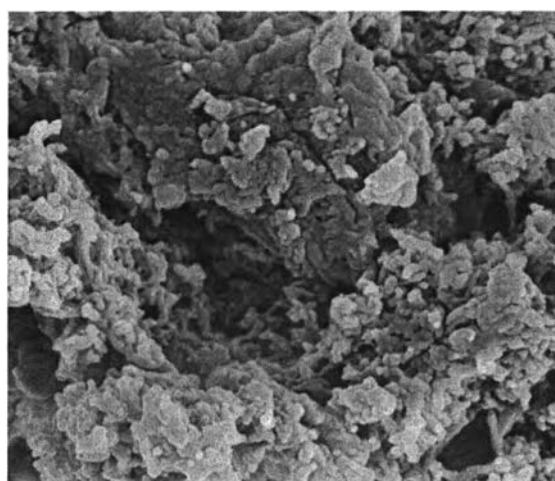
Figure G2 Morphology of 30:1 dPPPpatricle (15 kV, magnification of 20 kX).

For PCL and PPP/PCL composite, cross-section mode was employed to investigate a dispersion of PPP and PCL matrix. First, the sample was fractured in liquid nitrogen by forceps and stuck with a stub by carbon tape.Figure G4 show a good dispersion of PPP in PCL.
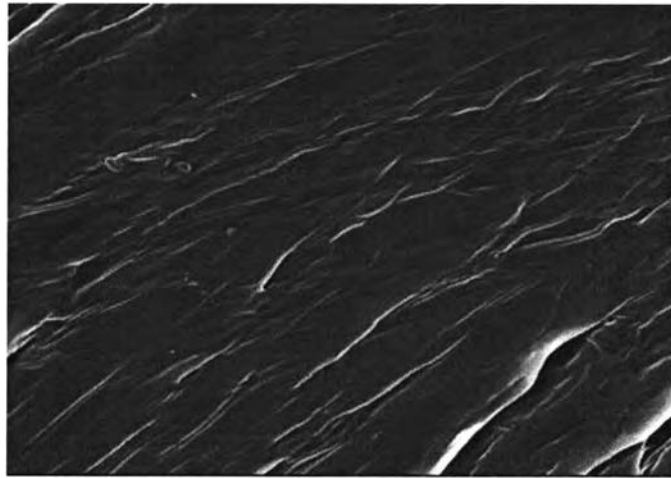
Figure G3 Morphology of neat PCL (15 kV, magnification of 1.5 kX).
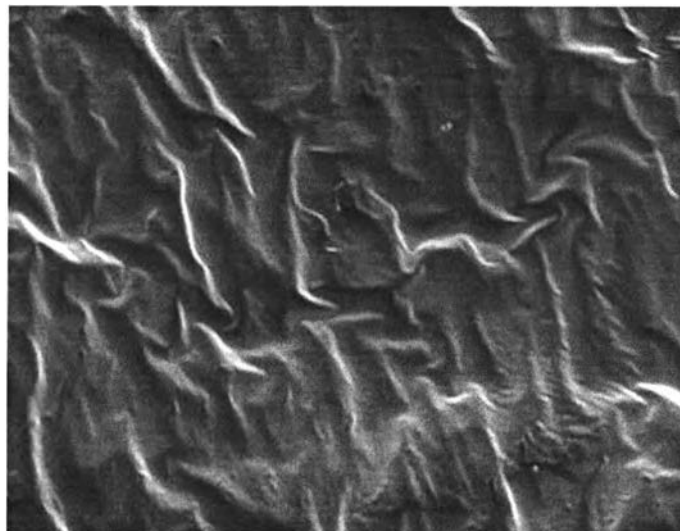
Figure G4 Morphology of 3%wt BPO cPCL (15 kV, magnification of 1.5 kX).
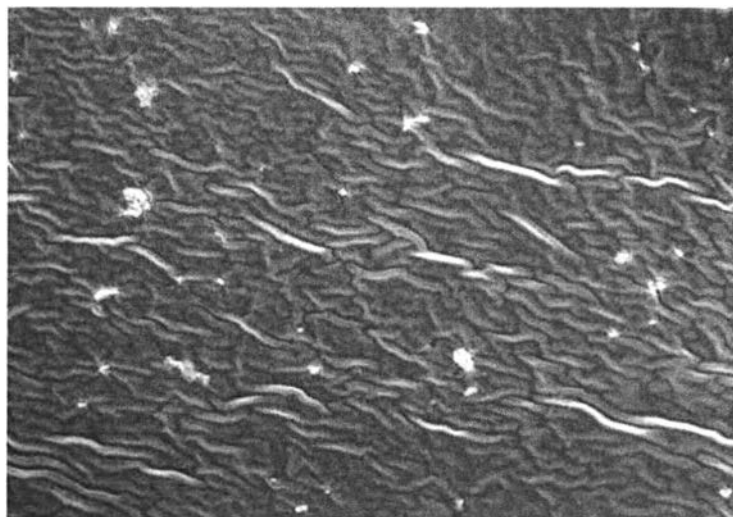
Figure G4 Morphology of 1%v/v 30:1 dPPP/3%wt BPO cPCL (15 kV, magnification of 0.5 kX).

Appendix H Investigation of crosslinking efficiency of PCL

Benzoyl peroxide (BPO) can be used to crosslink PCL via radical crosslinking to increase the mechanical properties. Swelling test was done to investigate crosslinking efficiency of PCL and the important factor is percentage of gel fraction (%G) which can be calculated by the equation H1:

$$\%G = m_d/m_0 \times 100 \tag{H1}$$

The percentage of swelling was calculated according to the following equation H2:

$$\% \text{ swelling} = (m_s - m_d)/m_d \times 100 \tag{H2}$$

The percentage of weight loss was calculated according to the following equation H3:

$$\% \text{ weight loss} = (m_0 - m_d)/m_d \times 100 \tag{H3}$$

when m_0, m_s and m_d are an initial weight of the sample before doing the test, The mass of the swollen specimen at equilibrium and the weight of dried sample after the test respectively.

Casted PCL film from uncured, 1%wt, 3%wt, 5%wt, 7%wt to 10%wt BPO, was cut into a rectangular shape with the dimension of 0.5x1 cm. The sample was weighted for measured m_0 and immersed in 5 cm^3 of benzene for 72 hours which was completely swelled. Then, the sample was collected and weighted again to measurem$_s$. Finally, the sample was placed in the presence of air for 72 hours to completely evaporated benzene and weighted again for investigate m_d. The experiment was operated at 25 °C. The result shows that 3%wt BPO crosslinked PCL has the highest % gel fraction corresponding to the highest crosslinking efficiency respectively. At the higher concentration of BPO, the % gel fraction is slightly dropped. This can be explained that the overabundant BPO can cause chain scission of PCL.Shorter PCL chain will be obtained by the C-H fragmentation. In

addition,CO and CO_2 can be generated by the C-O and C=O fragmentation. According to these reasons, the molecular weight of PCL is decreased.

Table H1 Raw data of swelling test at various BPO concentration

Concentration of BPO	m_0 (g)	m_s(g)	m_d (g)	% swelling	% weight loss	% gel fraction
1%wt BPO I	0.0128	0.1782	0.0051	3,394.12	150.98	39.84
II	0.0154	0.1880	0.0048	3,816.67	220.83	31.16
III	0.0173	0.1531	0.0056	2,633.93	208.93	32.36
3%wt BPO I	0.0237	0.1945	0.0212	817.45	11.79	89.45
II	0.0281	0.2152	0.0256	740.62	9.77	91.10
III	0.0225	0.1878	0.0191	883.25	17.80	84.89
5%wt BPO I	0.0207	0.1381	0.0156	785.26	32.69	75.36
II	0.0178	0.1346	0.0125	976.80	42.40	70.22
III	0.0226	0.1492	0.0164	809.76	37.80	72.57
7%wt BPO I	0.0274	0.1414	0.0188	652.13	45.74	68.61
II	0.0297	0.1623	0.0201	707.46	47.76	67.67
III	0.0266	0.1479	0.0183	708.19	45.36	68.79
10%wt BPO I	0.0192	0.0891	0.0108	725.00	77.78	56.25
II	0.0206	0.0934	0.0132	607.57	56.06	64.07
III	0.0211	0.0909	0.0129	604.65	63.57	61.14

Table H2 The average %gel fraction at various BPO concentration

Concentration of BPO	% gel fraction (average)	Standard deviation
1%wt BPO	34.45	3.84
3%wt BPO	88.48	3.22
5%wt BPO	72.72	2.57
7%wt BPO	68.34	0.60
10%wt BPO	60.49	3.95
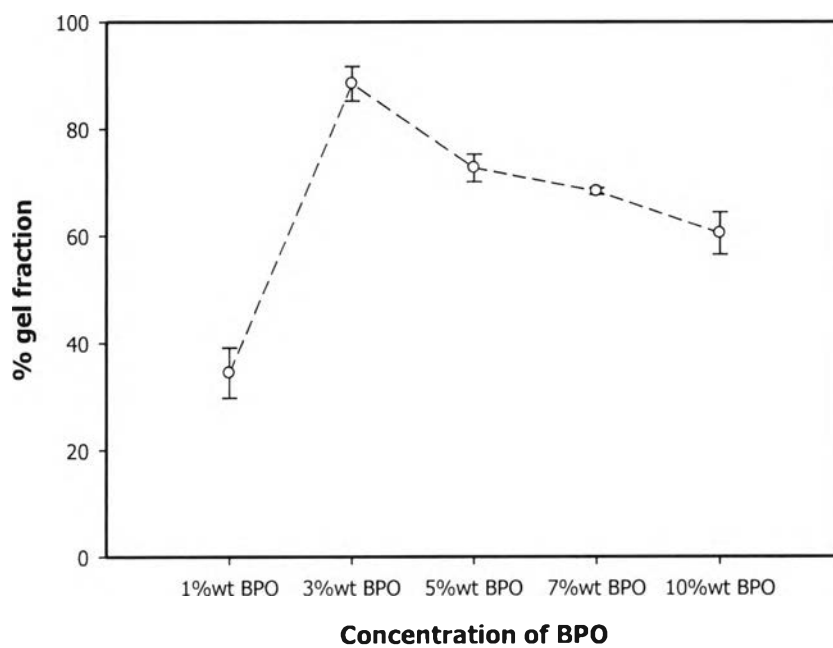
Figure H1 The comparison of % gel fraction at various BPO concentration.

Appendix I Electromechanical Properties of Poly(ε-caprolactone)(PCL) Film at Various Crosslinking Ratio

Electrorheological properties of uncrosslink and crosslinked PCL film strength were investigated by the melt rheometer (Rheometric Scientific, ARES) which a DC voltage was applied by a DC power supply(Instek, 8216A) which can provide a constant electric field to 2 kV/mm. An input voltage was monitored by a digital multimeter (Tektronix, CDM250).Dynamic strain sweep test were investigeated firstly to determine a linear viscoelastic regime, shown on these following figures.
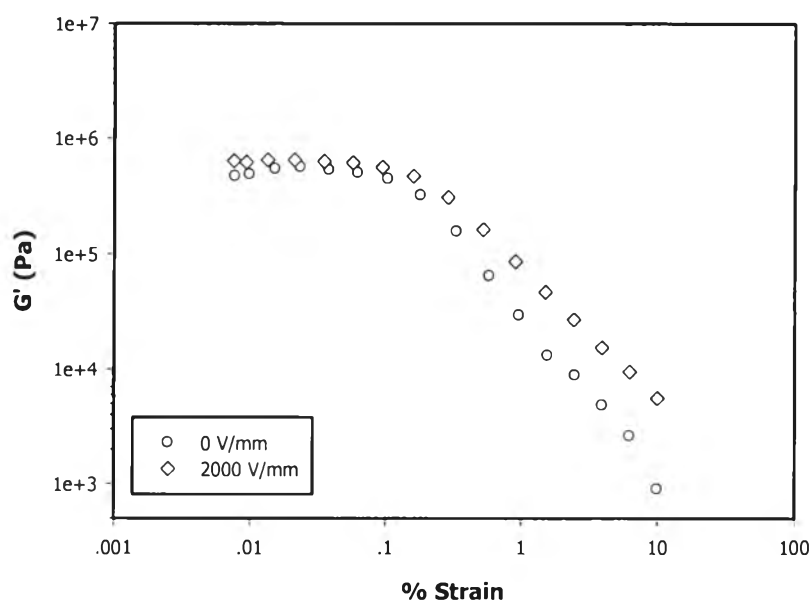
Figure I1 Dynamic strain sweep test of neat PCL (% strain from 0.01 to 10, film thickness 0.542 mm, 25°C).
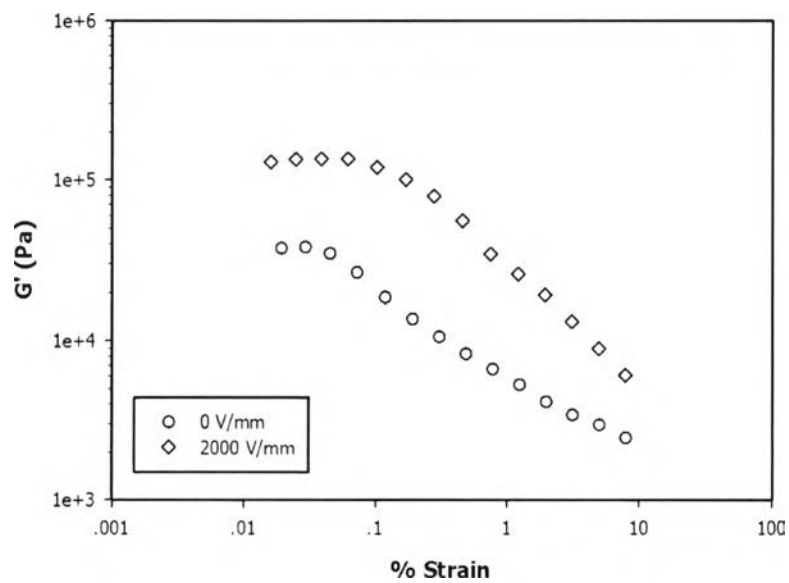
Figure I2 Dynamic strain sweep test of 1%wt BPO crosslinked PCL (% strain from 0.01 to 10, film thickness 0.443 mm,25°C).
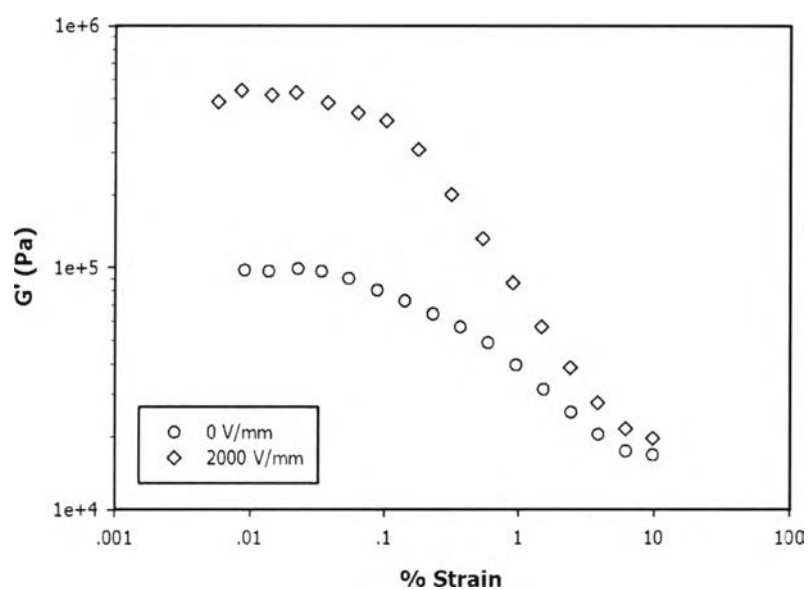
Figure I3 Dynamic strain sweep test of 3%wt BPO crosslinked PCL (% strain from 0.01 to 10, film thickness 0.584 mm,25°C).
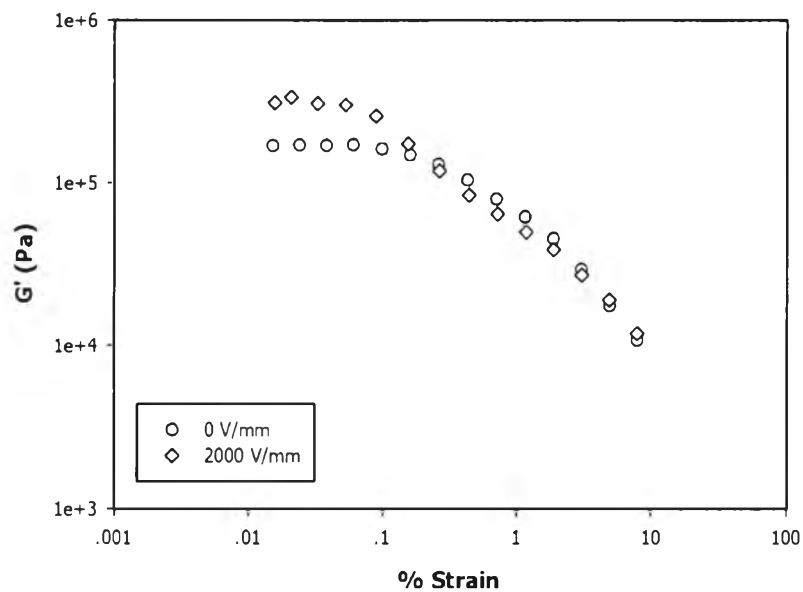
Figure I4 Dynamic strain sweep test of 5%wt BPO crosslinked PCL (% strain from 0.01 to 10,film thickness 0.461 mm,25°C).
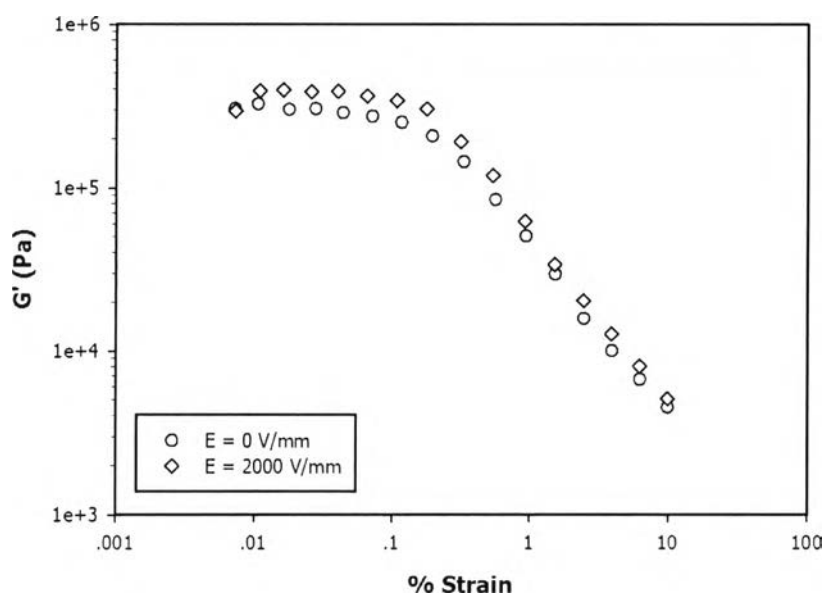
Figure I5 Dynamic strain sweep test of 7%wt BPO crosslinked PCL (% strain from 0.01 to 10,film thickness 0.474 mm,25°C).
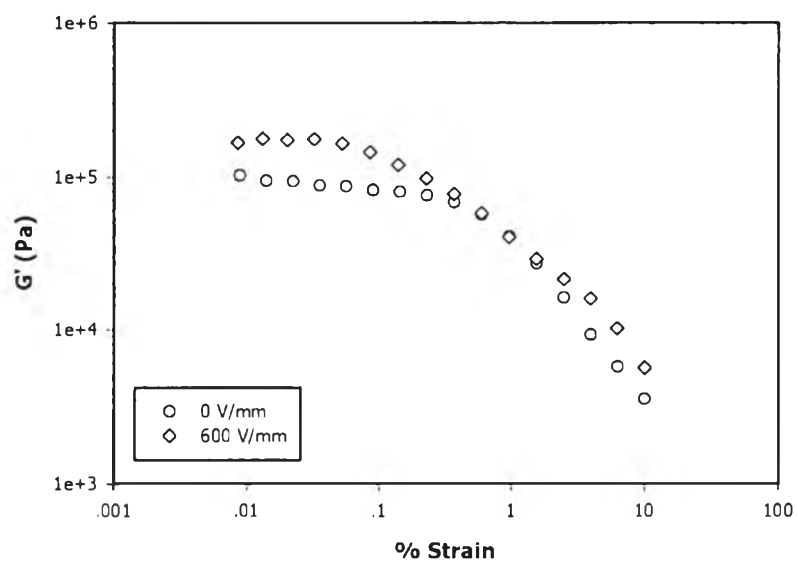
Figure I6 Dynamic strain sweep test of 10%wt BPO crosslinked PCL (% strain from 0.01 to 10,film thickness 0.566 mm,25°C).

A dynamic frequency sweep test was carried out with an applied electric field from 0 to 2000 kV. Storage modulus(G') of each sample was investigated as a function of frequency from 0.1 to 100 rad/s, at the %strain of 0.03.
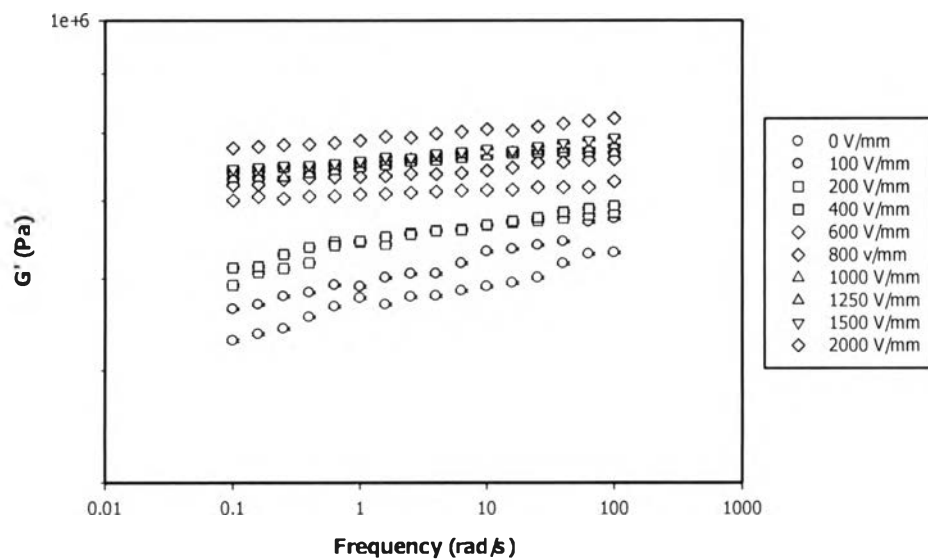
Figure I7 Dynamic frequency sweep test of neat PCL (frequency from 0.1 to 100 rad/s, %strain 0.03,film thickness 0.542 mm,25°C).
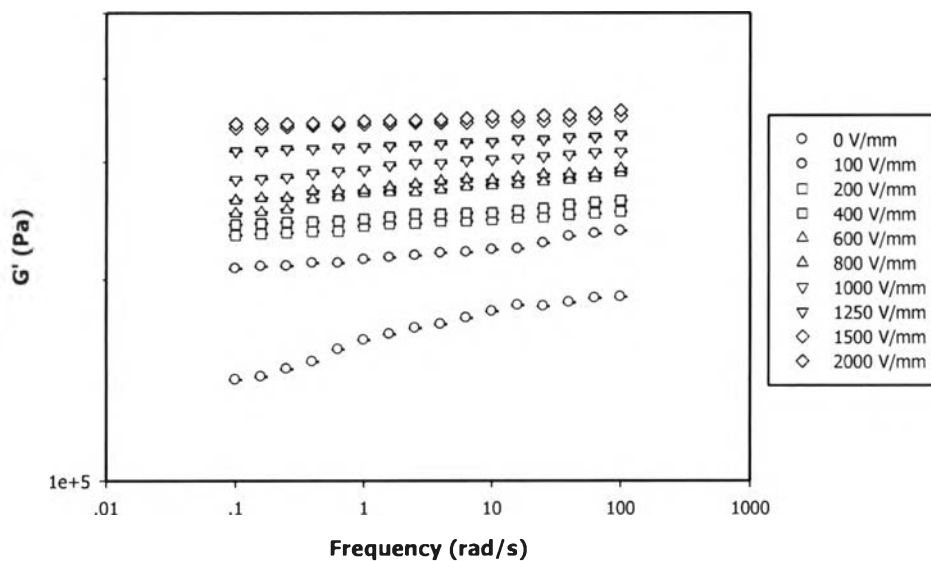
Figure I8 Dynamic frequency sweep test of 1%wt BPO crosslinked PCL (frequency from 0.1 to 100 rad/s, %strain 0.03,film thickness 0.443 mm,25°C).
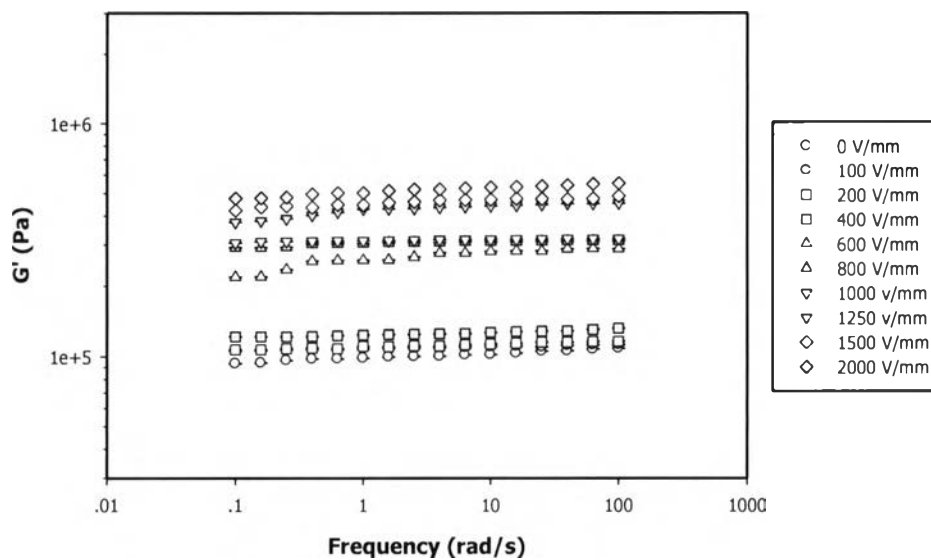
Figure I9 Dynamic frequency sweep test of 3%wt BPO crosslinked PCL (frequency from 0.1 to 100 rad/s, %strain 0.03,film thickness 0.584 mm,25°C).
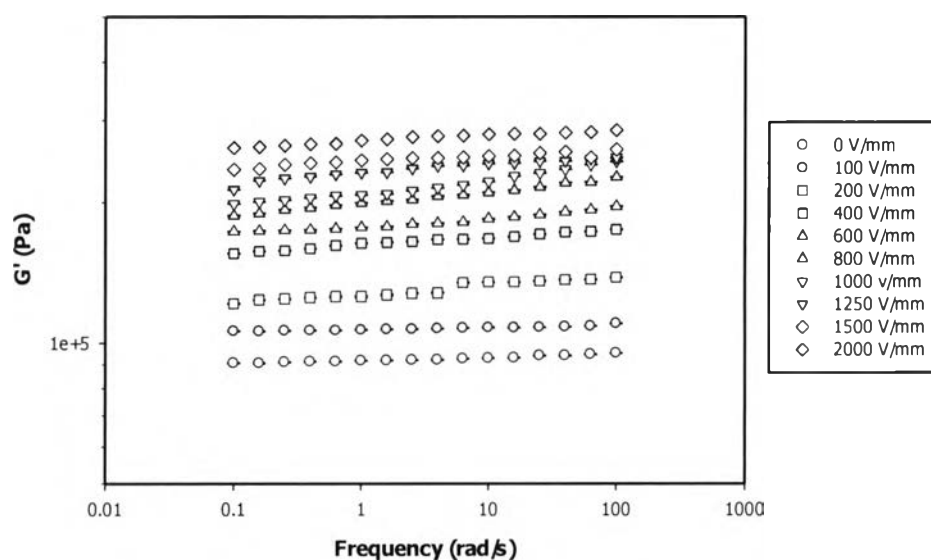
Figure I10 Dynamic frequency sweep test of 5%wt BPO crosslinked PCL (frequency from 0.1 to 100 rad/s, %strain 0.03,film thickness 0.461 mm,25°C).
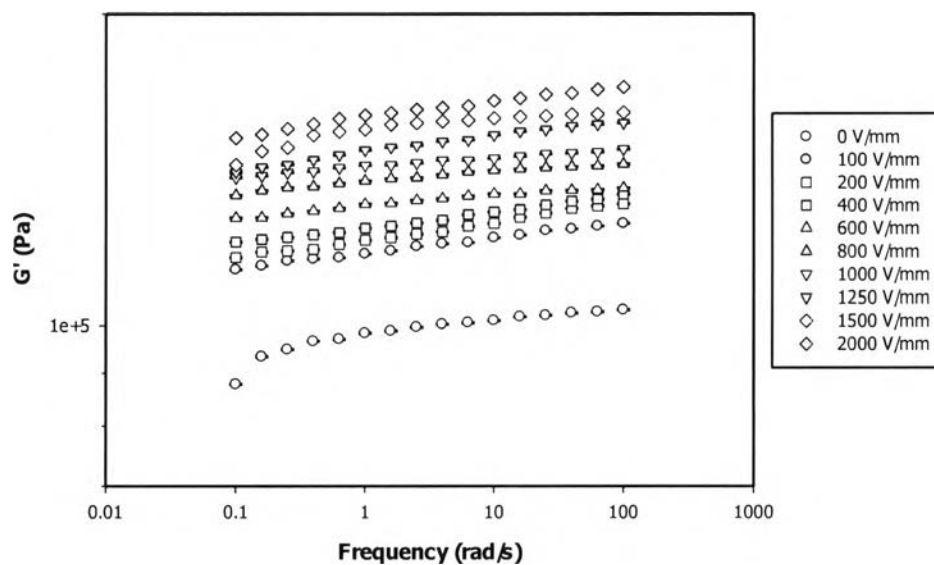
Figure I11   Dynamic frequency sweep test of 7%wt BPO crosslinked PCL (frequency from 0.1 to 100 rad/s, %strain 0.03,film thickness 0.474 mm,25°C).
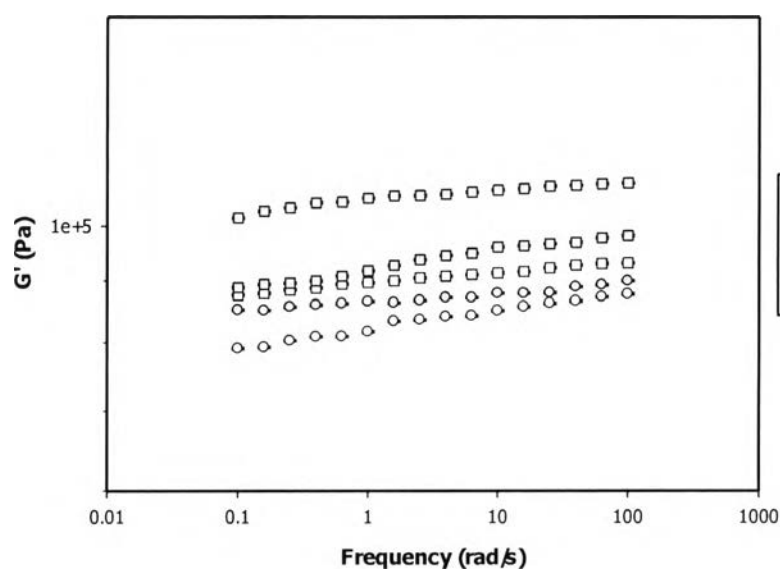
Figure I12   Dynamic frequency sweep test of 10%wt BPO crosslinked PCL (frequency from 0.1 to 100 rad/s, %strain 0.03,film thickness 0.566 mm,25°C).

Temporal response of each sample was figure out by time sweep test which an applied electric field wason and off alternatively. The G′ at steady state and stotage modulus response in the presence of electric field of each sample was investigated as a function of time from 0 to 5000 s, at the frequency of 1 rad/s.
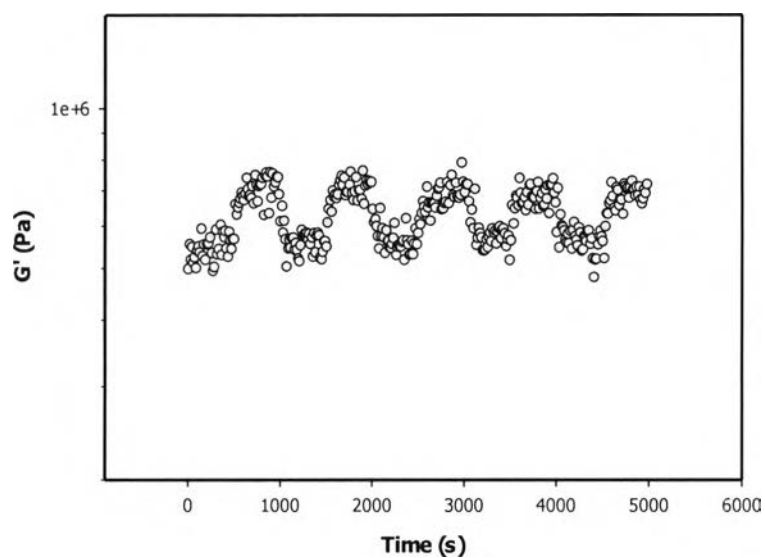
Figure I13 Temporal response of neatPCL (%strain 0.03, electric field strength of 2 kV, frequency 1 rad/s,film thickness 0.542 mm,25°C).
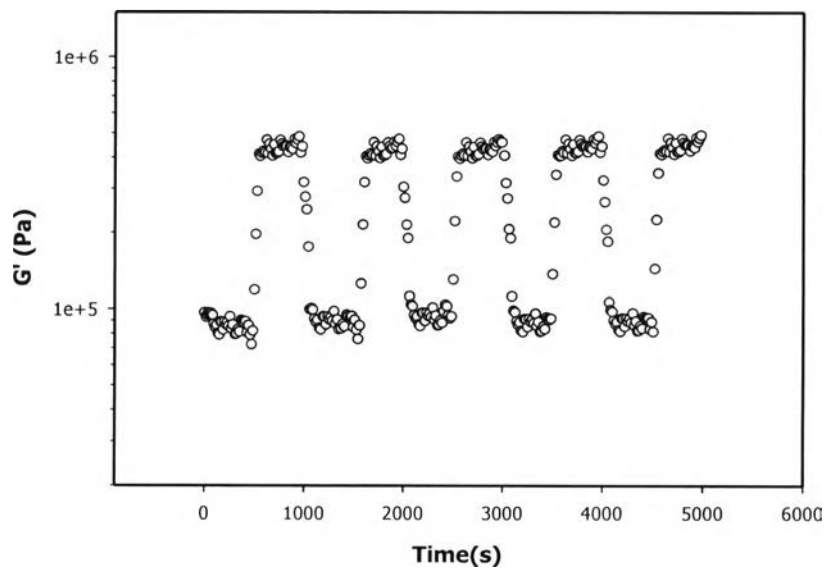
Figure I14 Temporal response of 3%wt BPO crosslinked PCL (%strain 0.03, electric field strength of 2 kV, frequency 1 rad/s,film thickness 0.443 mm,25°C).
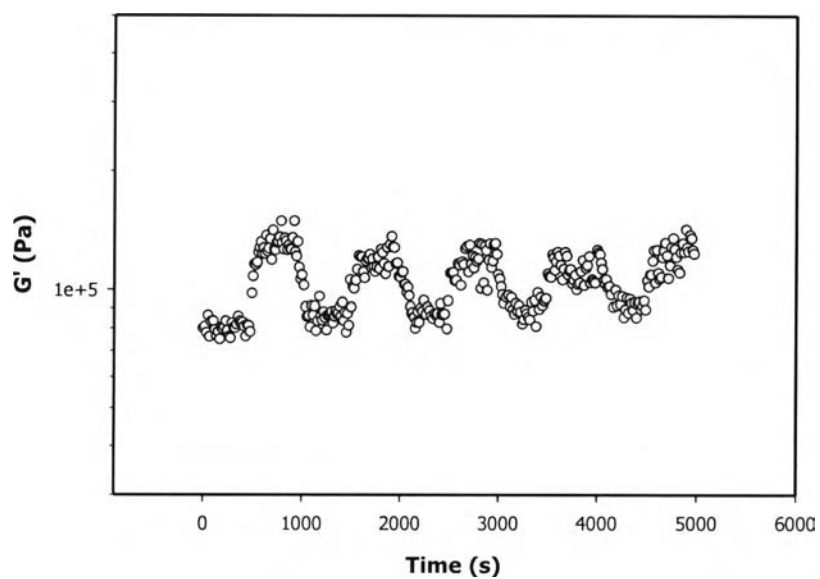
Figure I15 Temporal response of 10%wt BPO crosslinked PCL (%strain 0.03, electric field strength of 0.6 kV, frequency 1 rad/s,film thickness 0.566 mm,25°C).
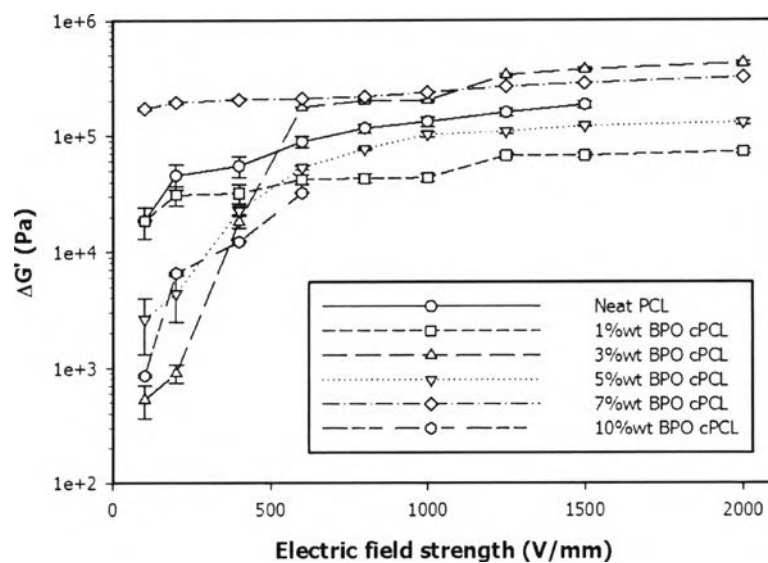
Figure I16 The comparison of storage modulus response ($\Delta G'$) as a function of electric field strength of PCL and crosslinked PCL film at each crosslinking ratio.
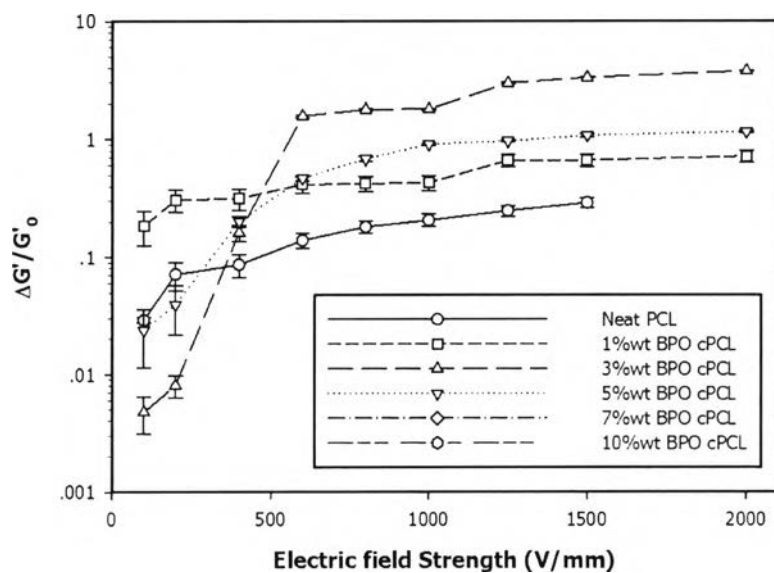
Figure I17 The comparison of storage modulus sensitivity($\Delta G'/G'_0$) as a function of electric field strength of PCL and crosslinked PCL film at each crosslinking ratio.

The initial storage modulus (G'_0) of the PCL films decreases when increasing BPO concentration. This is because of the packing of crystalline is restricted by the crosslinking agent in the casting procedure, corresponding to the reduction of the crystalline region. The higher concentration of BPO, the less crystalline regionis generated in the sample.
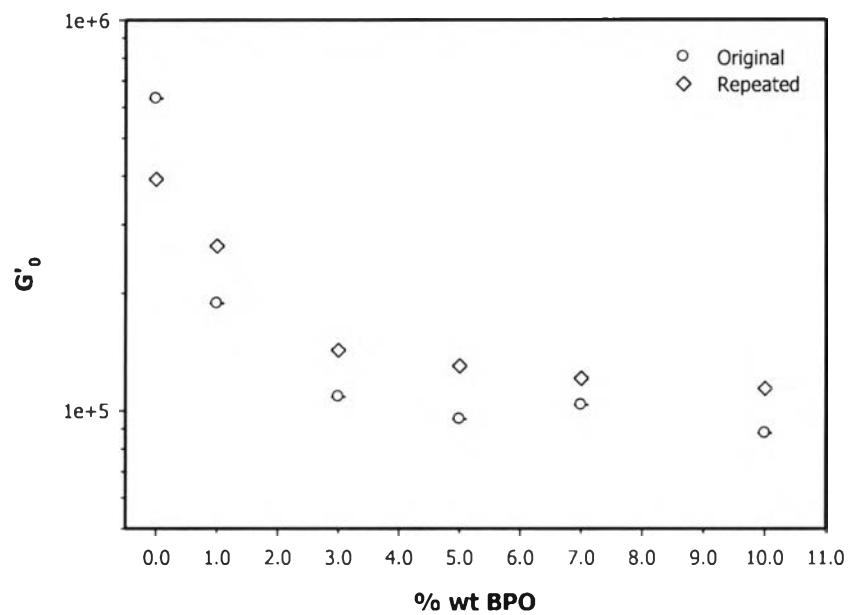

**Figure I18** The initial storage modulus (G'_0) at various BPO concentration.

Appendix J Electromechanical Properties of Poly(p-phenylene) (PPP)/Poly(ε-caprolactone) (PCL)Composite at Various Doping Level

Influence of doping level on electromechanical properties of PPP/PCL composite were investigated by the melt rheometer (Rheometric Scientific, Ares) in which a DC voltage was applied by a DC power supply(Instek, 8216A) which can provide a constant electric field up to 2 kV/mm. An input voltage was monitored by a digital multimeter(Tektronix, CDM250).In this study, 1%v/v of PPP was fixed for each doping level and embedded into PCL matrix. First, dynamic strain sweep test were investigeated to determine a linear viscoelastic regime.
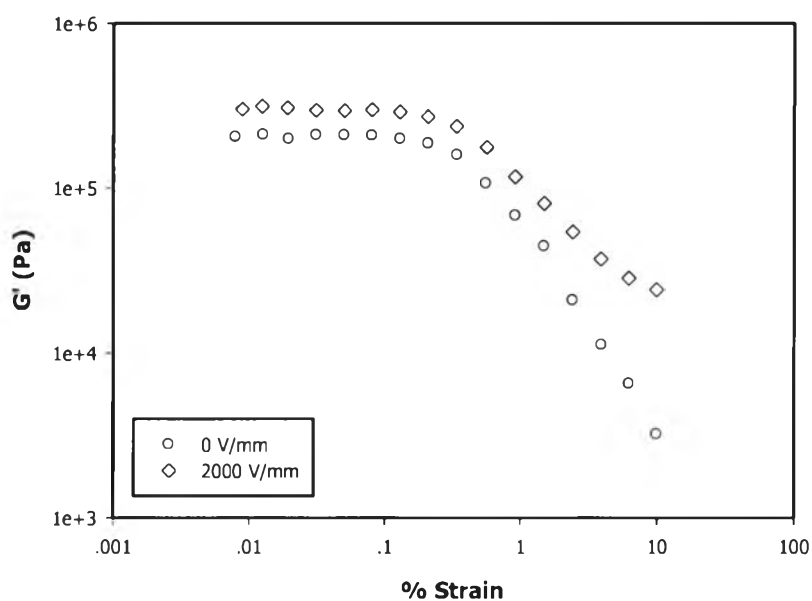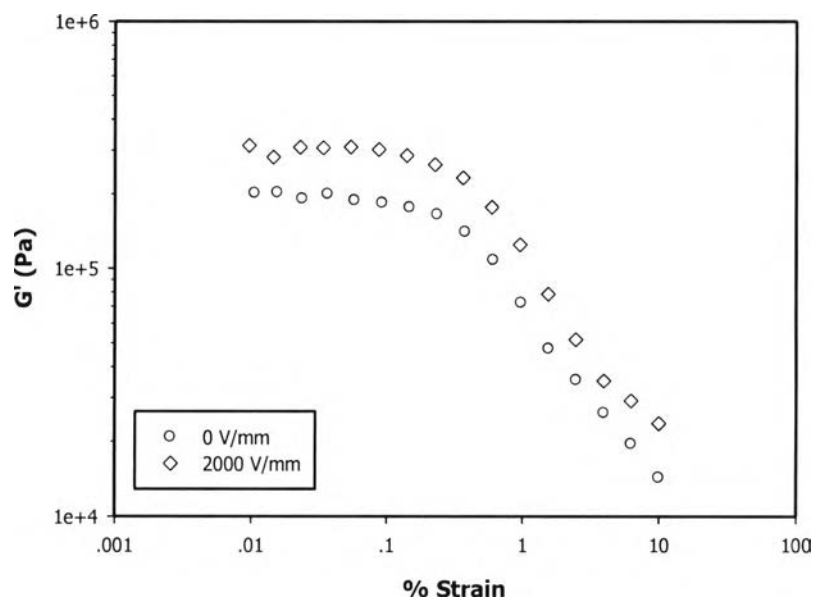

Figure J1 Dynamic strain sweep test of 1%v/v uPPP/3%wt BPO cPCL (% strain from 0.01 to 10, film thickness 0.724 mm,25°C).
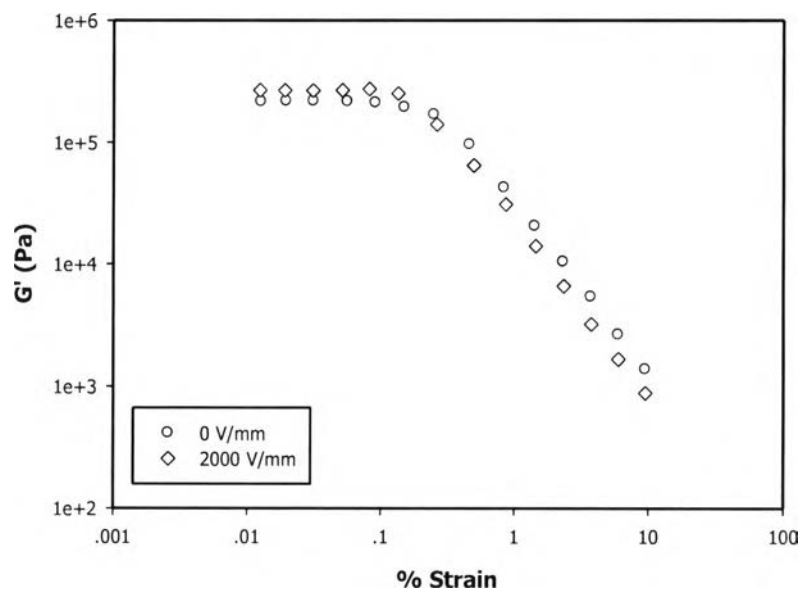
Figure J2 Dynamic strain sweep test of 1% v/v 1:30 dPPP/3%wt BPO cPCL (% strain from 0.01 to 10,film thickness 0.583 mm, 25°C).
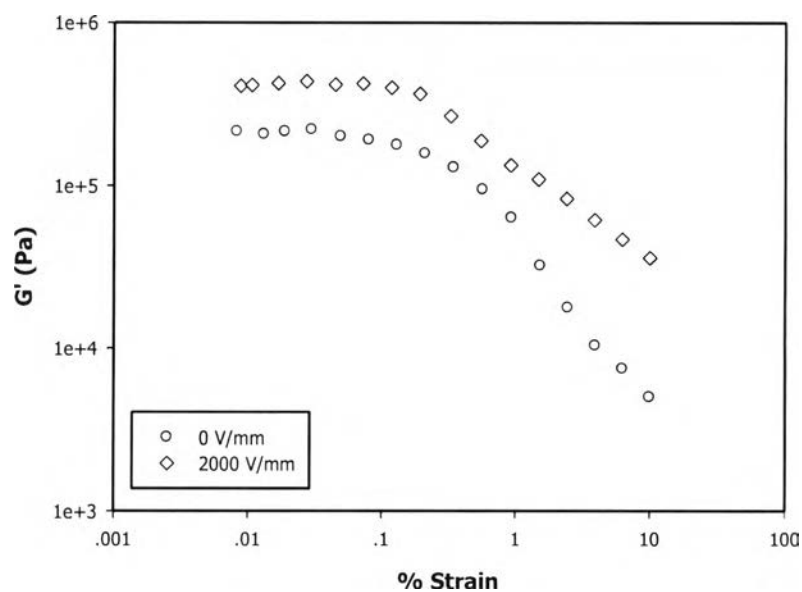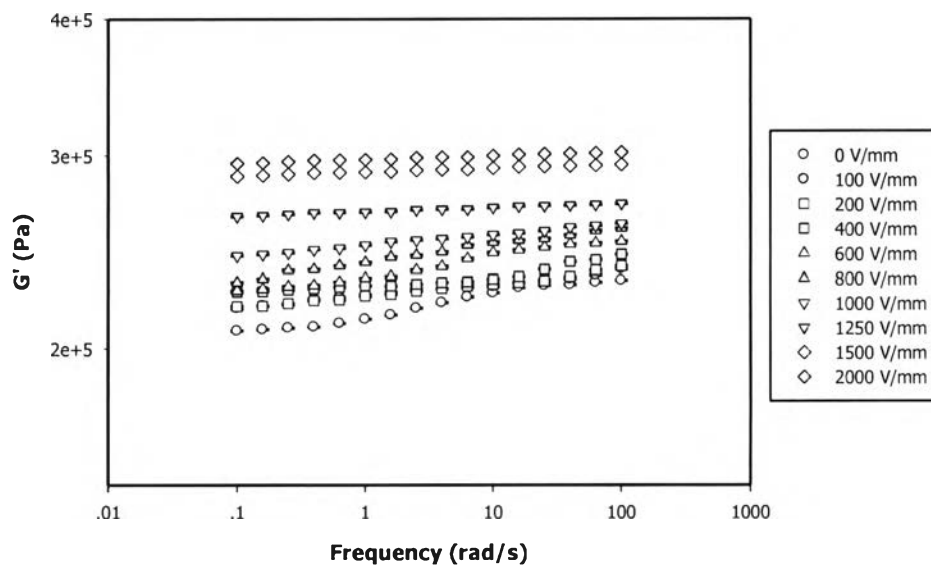

Figure J3 Dynamic strain sweep test of 1% v/v 30:1 dPPP/3%wt BPO cPCL (% strain from 0.01 to 10, film thickness 0.645 mm, 25°C).
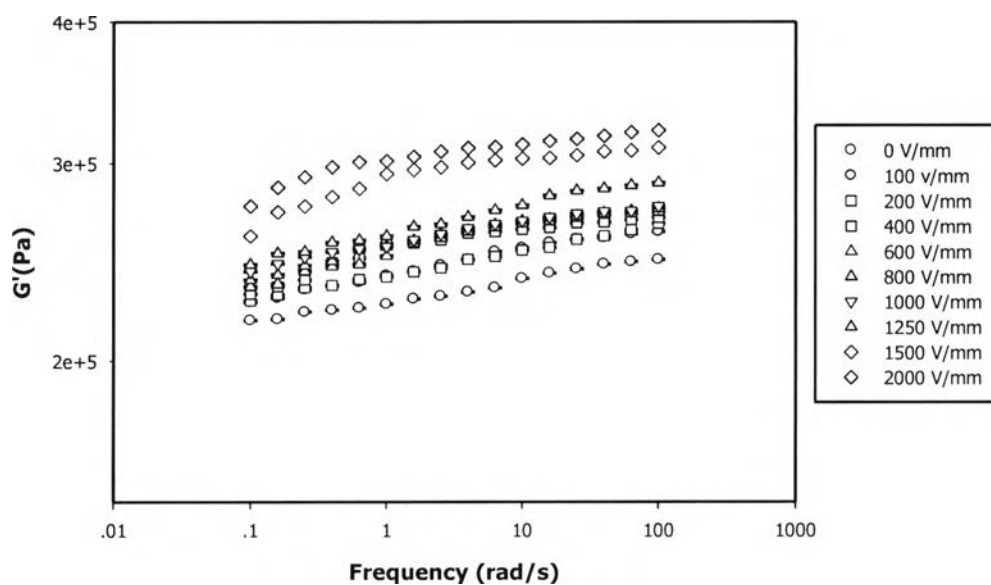
Figure J4 Dynamic strain sweep test of 1% v/v 100:1 dPPP/3%wt BPO cPCL (% strain from 0.01 to 10,film thickness 0.797 mm, 25°C).
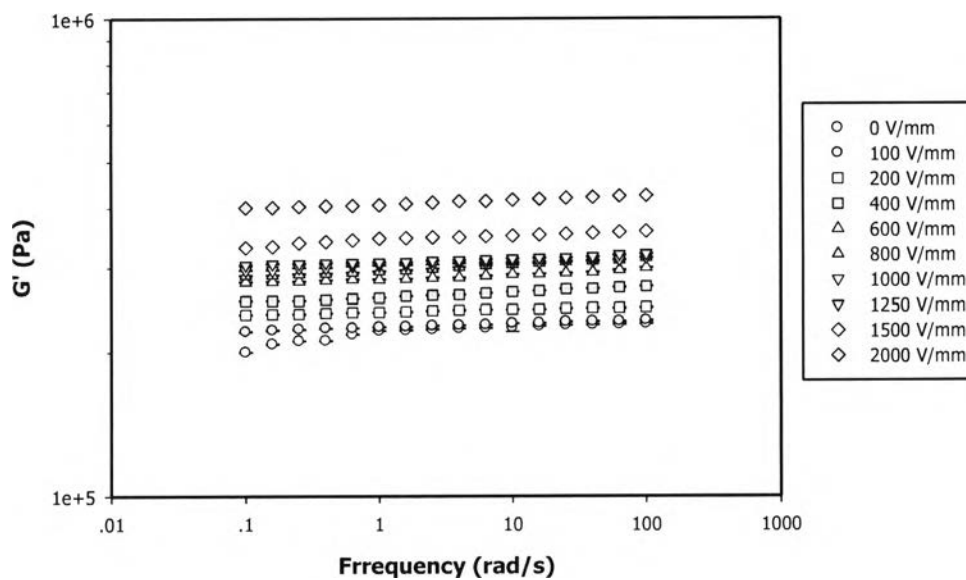
A dynamic frequency sweep test was carried out with an applied electric field from 0 to 2 kV. Storage modulus(G′) of each sample was investigated as a function of frequency from 0.1 to 100 rad/s, at the %strain of 0.03.
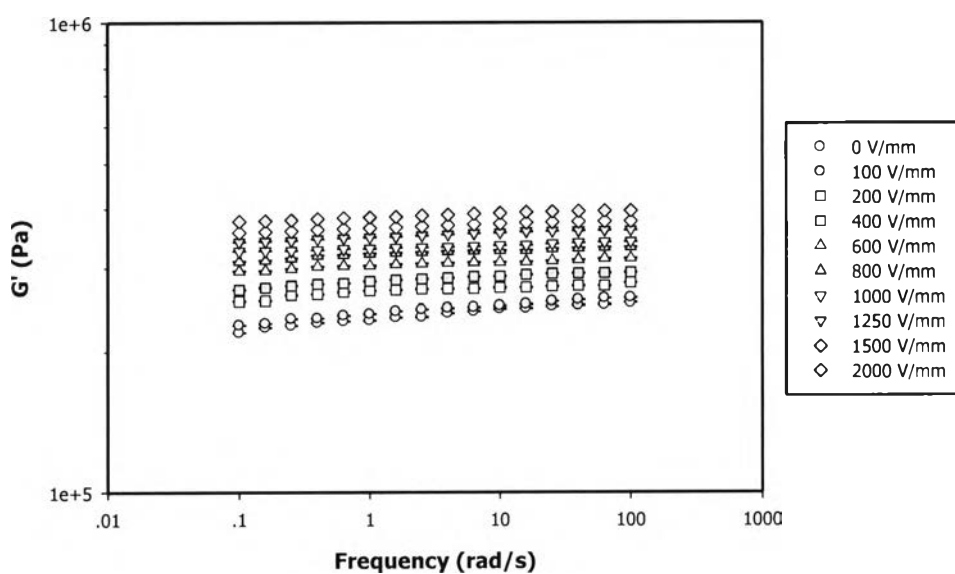
Figure J5 Dynamic frequency sweep test of 1%v/v uPPP/3%wt BPO cPCL (frequency from 0.1 to 100 rad/s, %strain 0.03,film thickness 0.724 mm, 25°C).

Figure J6 Dynamic frequency sweep test of 1%v/v 1:30 dPPP/3%wt BPO cPCL (frequency from 0.1 to 100 rad/s, %strain 0.03,film thickness 0.583 mm, 25°C).

Figure J7 Dynamic frequency sweep test of 1%v/v 30:1 dPPP/3%wt BPO cPCL (frequency from 0.1 to 100 rad/s, %strain 0.03,film thickness 0.645 mm, 25°C).


Figure J8 Dynamic frequency sweep test of 1%v/v 100:1 dPPP/3%wt BPO cPCL (frequency from 0.1 to 100 rad/s, %strain 0.03, film thickness 0.797 mm, 25°C).

Temporal response of each sample was figure out by time sweep test which an aplied electric field wason and off alternatively. The G′ at steady state and storage modulus response in the presence of electric field of each sample was investigated as a function of time from 0 to 5000 s at the frequency of 1 rad/s.
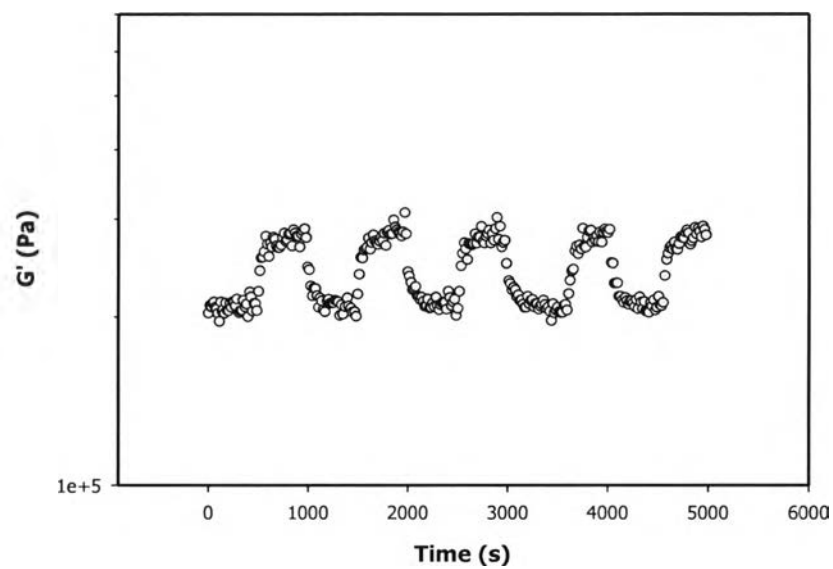
Figure J9 Temporal response of 1%v/v uPPP/3%wt BPO cPCL (%strain 0.03, electric field strength of 2 kV, film thickness 0.724, 25°C).
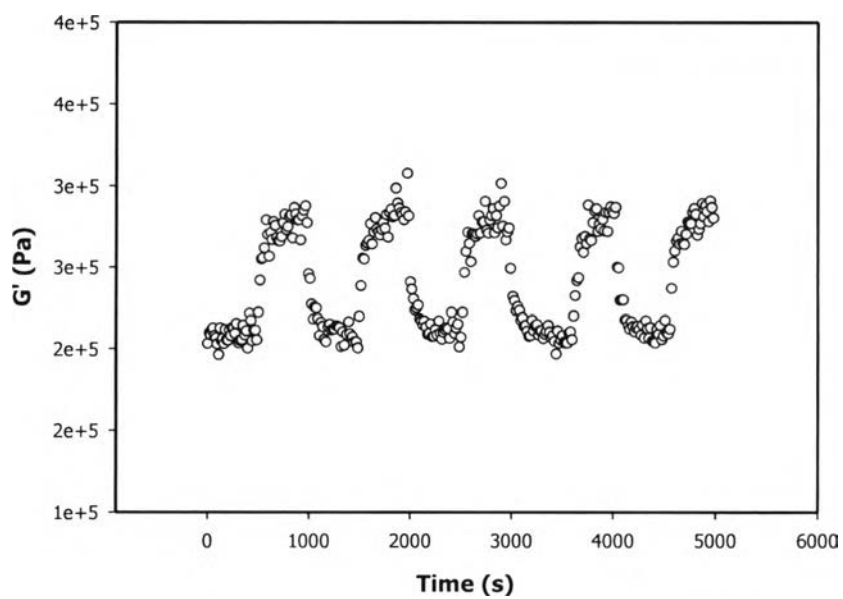
Figure J10 Temporal response of 1%v/v 1:30 dPPP/3%wt BPO cPCL (%strain 0.03, electric field strength of 2 kV,film thickness 0.583, 25°C).
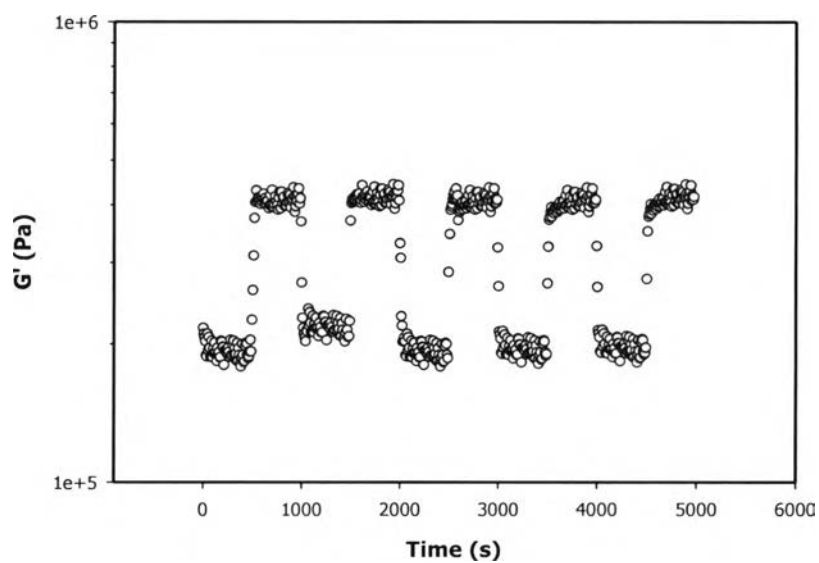
Figure J11 Temporal response of 1%v/v 30:1 dPPP/3%wt BPO cPCL (%strain 0.03, electric field strength of 2 kV,film thickness 0.645, 25°C).
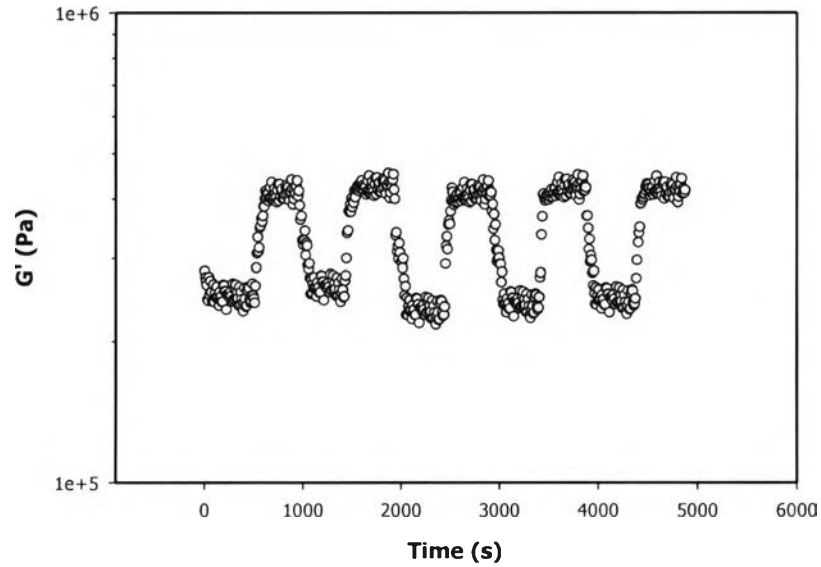
Figure J12 Temporal response of 1%v/v 100:1 dPPP/3%wt BPO cPCL (%strain 0.03,electric field strength of 2 kV, film thickness 0.797, 25°C).
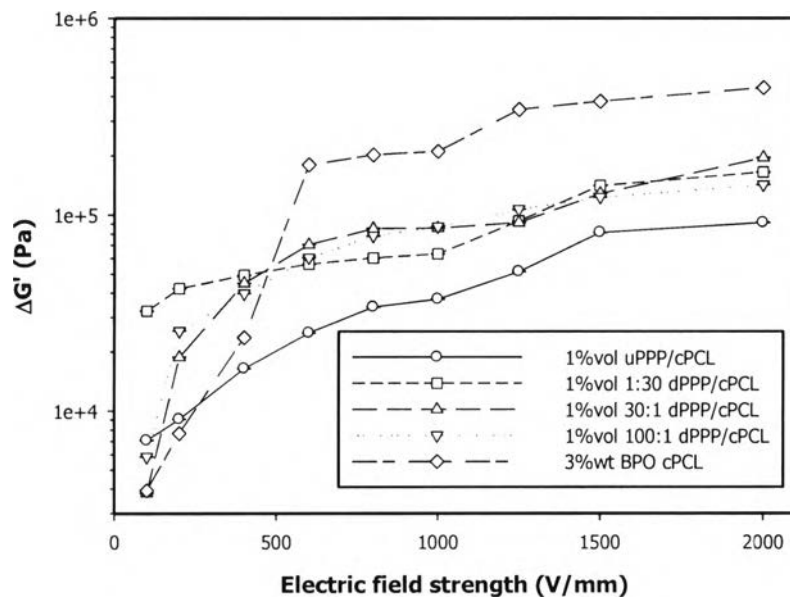
Figure J13 The comparison of storage modulus response ($\Delta G'$) as a function of electric field strength of PPP/PCL composite at each doping level.
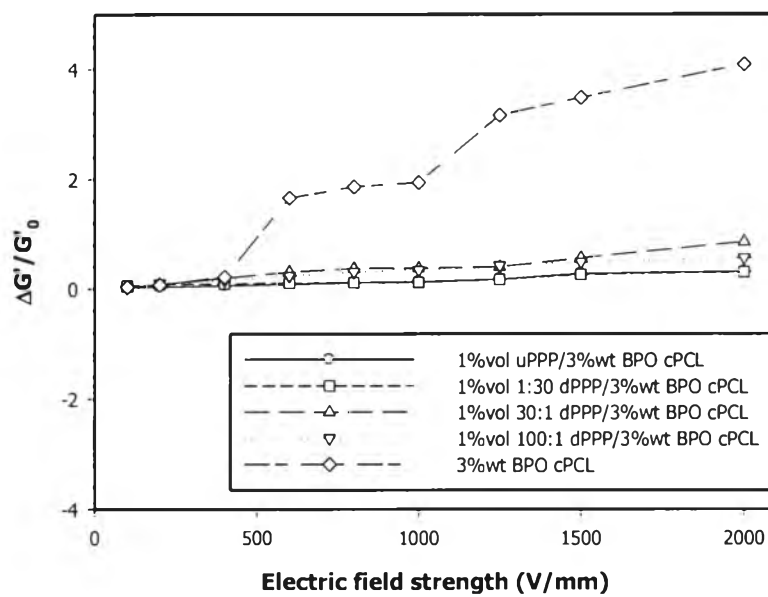
Figure J14 The comparison of storage modulus sensitivity($\Delta G'/G'_0$) as a function of electric field strength of PPP/PCL composite at each doping level.

Appendix K   Electromechanical Properties of Poly(p-phenylene) (PPP)/Poly(ε-caprolactone) (PCL)Composite at Various Concentration of Embedded PPP

Influence of concentration of embedded PPP on electromechanical properties of PPP/PCL composite were investigated by the melt rheometer (Rheometric Scientific, ARES) in which a DC voltage was applied by a DC power supply(Instek, 8216A) which can provide a constant electric field up to 2 kV/mm. An input voltage was monitored by a digital multimeter(Tektronix, CDM250). In this study, 30:1 dPPP and 3%wt BPO crosslinked PCL were chose to continue fabricating the composite because of the highest electrical sensitivity($\Delta G'/G'_0$). Dynamic strain sweep test were investigated firstly to determine a linear viscoelastic regime.
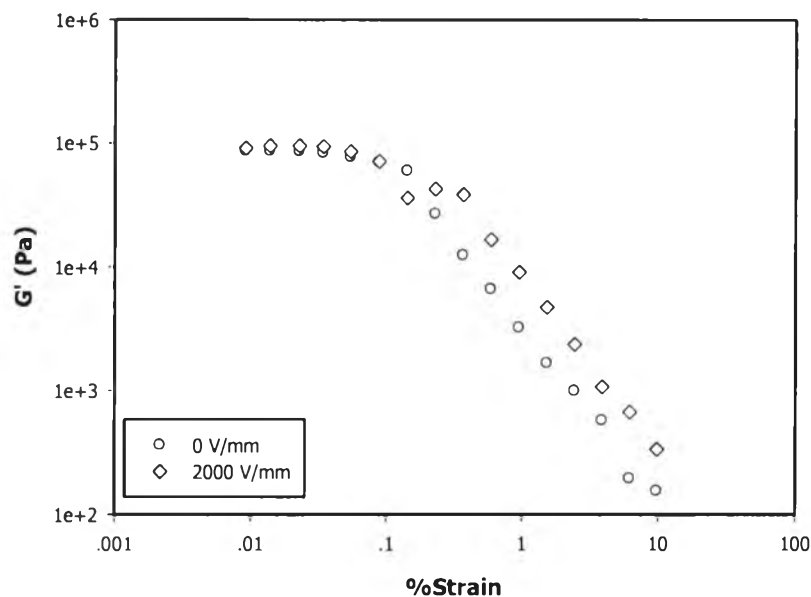
Figure K1 Dynamic strain sweep test of 0.01%v/v PPP/3% wt BPO cPCL(% strain from 0.01 to 10, film thickness 0.686 mm, 25 $^\circ$C).
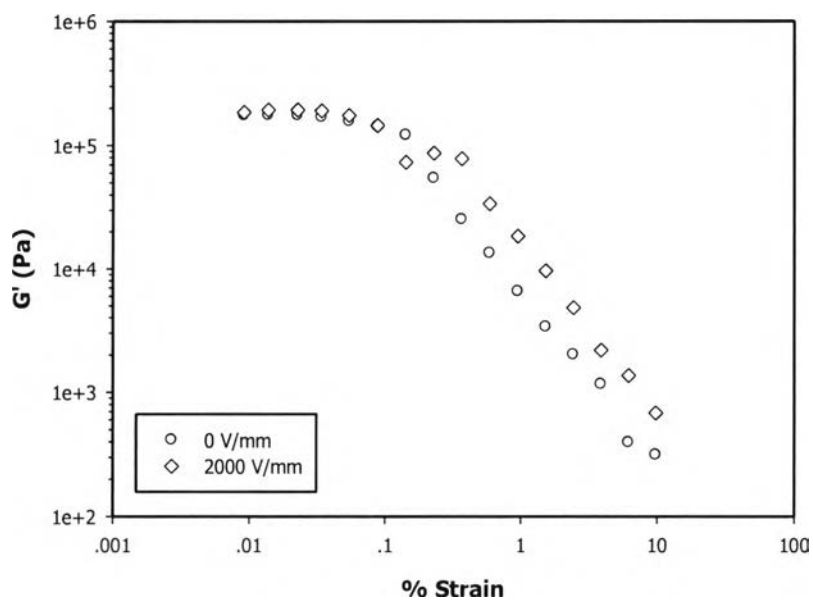
Figure K2 Dynamic strain sweep test of 0.05%v/v PPP/3% wt BPO cPCL(% strain from 0.01 to 10, film thickness 0.655 mm, 25 °C).
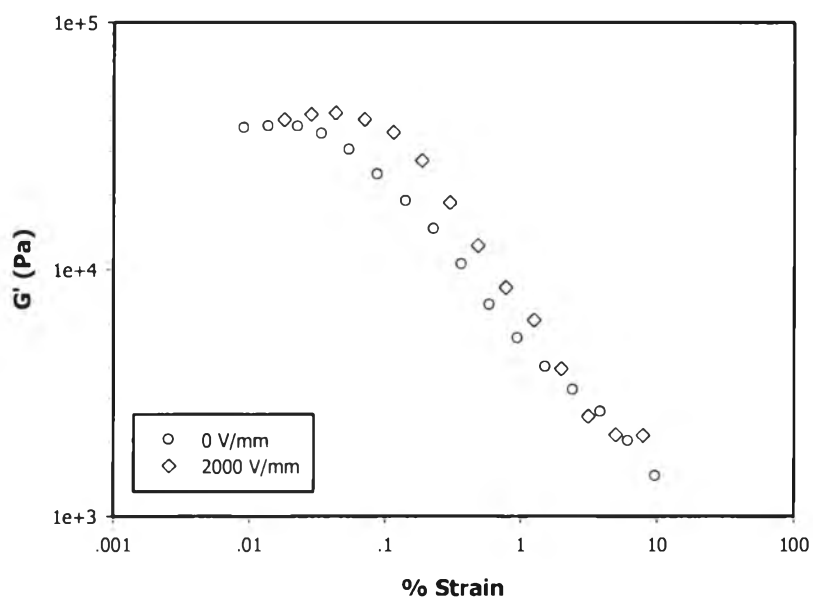
Figure K3 Dynamic strain sweep test of 0.1%v/v PPP/3% wt BPO cPCL(% strain from 0.01 to 10, film thickness 0.565 mm, 25°C).
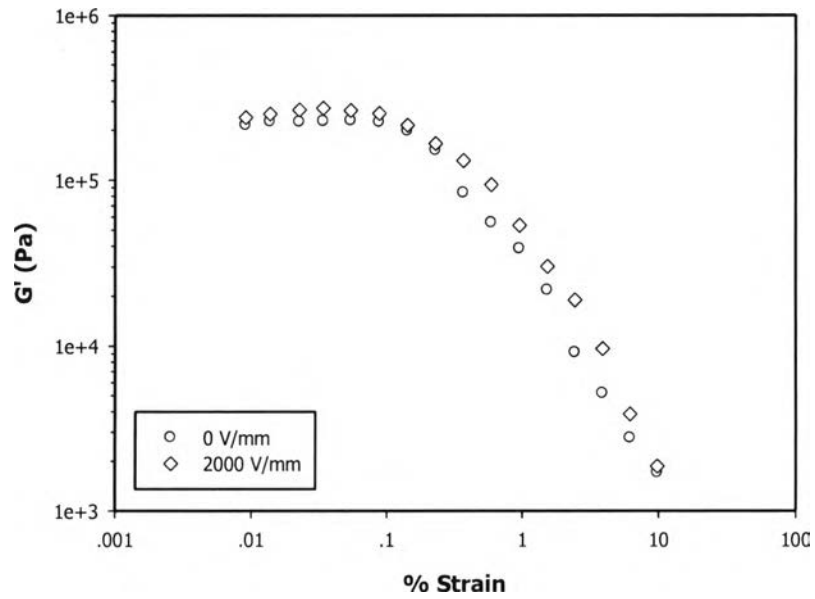
Figure K4 Dynamic strain sweep test of 0.5%v/v PPP/3% wt BPO cPCL(% strain from 0.01 to 10, film thickness 0.426 mm, 25°C).
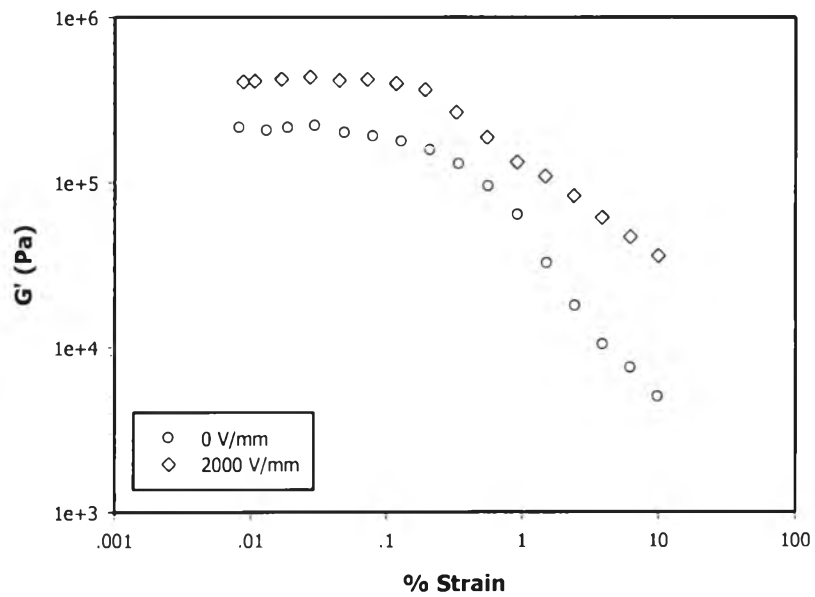
Figure K5 Dynamic strain sweep test of 1.0%v/v PPP/3% wt BPO cPCL(% strain from 0.01 to 10, film thickness 0.645 mm, 25°C).

A dynamic frequency sweep test was carried out with an applied electric field from 0 to 2kV. Storage modulus(G′) of each sample was investigated as a function of frequency from 0.1 to 100 rad/s, at the %strain of 0.03.
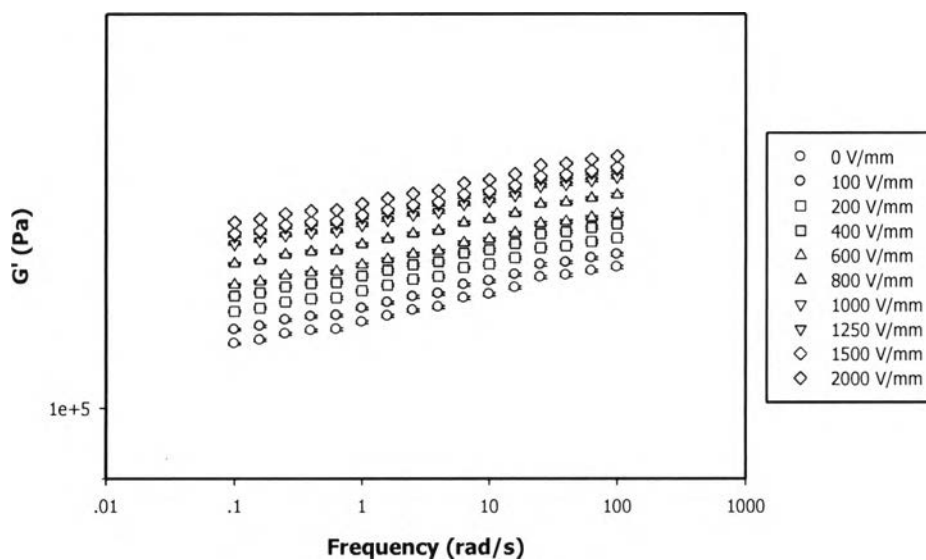
Figure K6 Dynamic frequency sweep test of 0.01%v/v 30:1 dPPP/3%wt BPO cPCL (frequency from 0.1 to 100 rad/s, %strain 0.03, film thickness 0.686 mm, 25 °C).
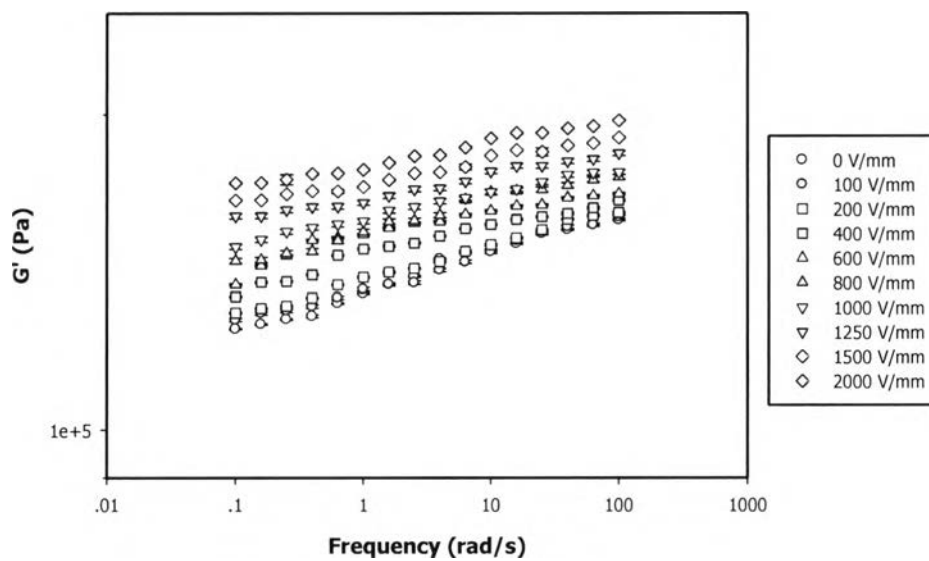
Figure K7 Dynamic frequency sweep test of 0.05% v/v 30:1 dPPP/3%wt BPO cPCL (frequency from 0.1 to 100 rad/s, %strain 0.03, film thickness 0.655 mm, 25°C).
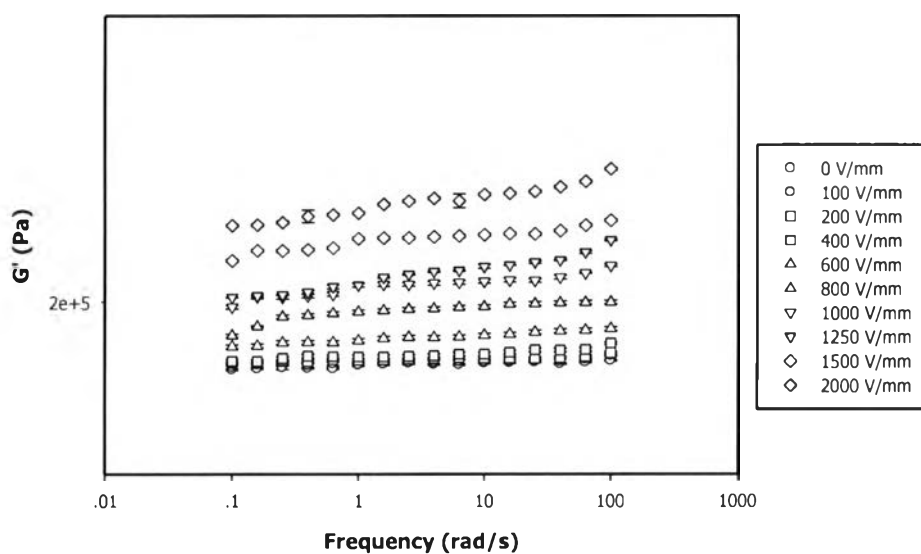
Figure K8 Dynamic frequency sweep test of 0.1%v/v 30:1 dPPP/3%wt BPO cPCL (frequency from 0.1 to 100 rad/s, %strain 0.03, film thickness 0.565 mm, 25°C).
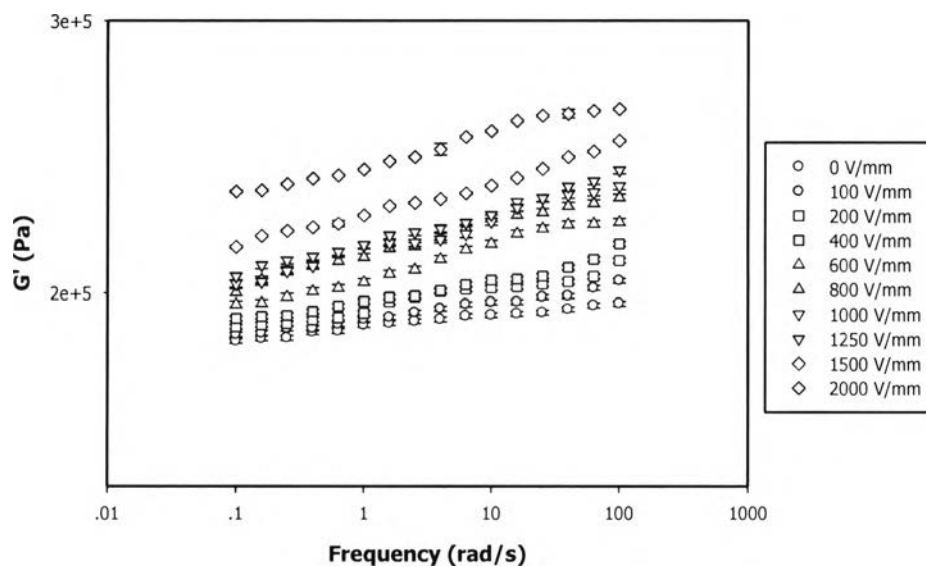
Figure K9 Dynamic frequency sweep test of 0.5%v/v 30:1 dPPP/3%wt BPO cPCL (frequency from 0.1 to 100 rad/s, %strain 0.03, film thickness 0.426 mm, 25°C).
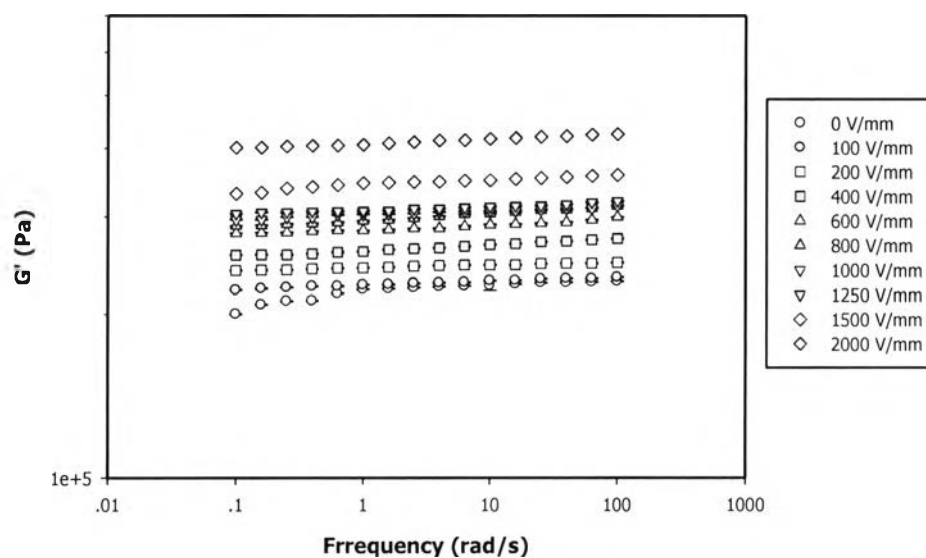
Figure K10 Dynamic frequency sweep test of 1.0%v/v 30:1 dPPP/3%wt BPO cPCL (frequency from 0.1 to 100 rad/s, %strain 0.03, film thickness 0.645 mm, 25°C).

Temporal response of each sample was figured out by time sweep test which an applied electric field wason and off alternatively. The G′ at steady state and

storage modulus response in the presence of electric field of each sample was investigated as a function of time from 0 to 5000 sat the frequency of 1 rad/s.
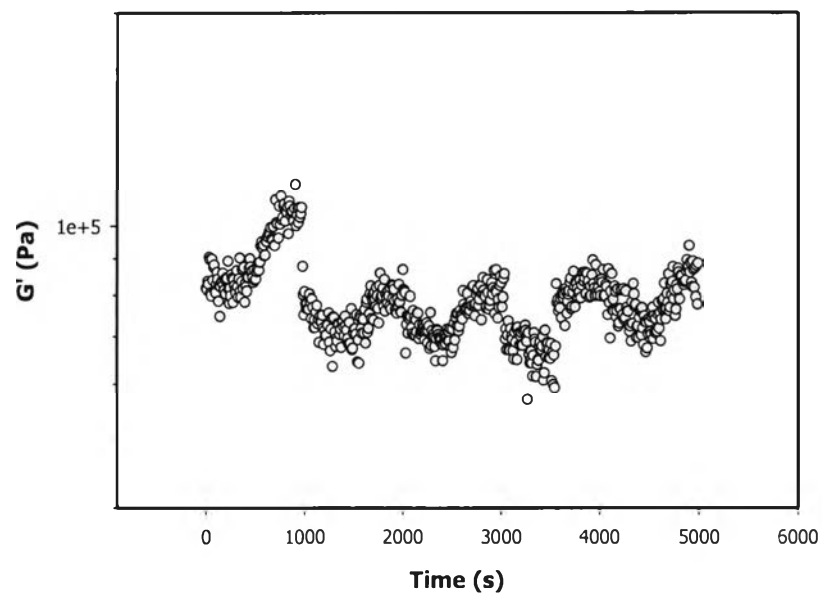
Figure K11 Temporal response of 0.01%v/v 30:1 dPPP/3%wt BPO cPCL(%strain 0.03, electric field strength of 2 kV, frequency 100 rad/s, film thickness 0.686 mm, 25°C).
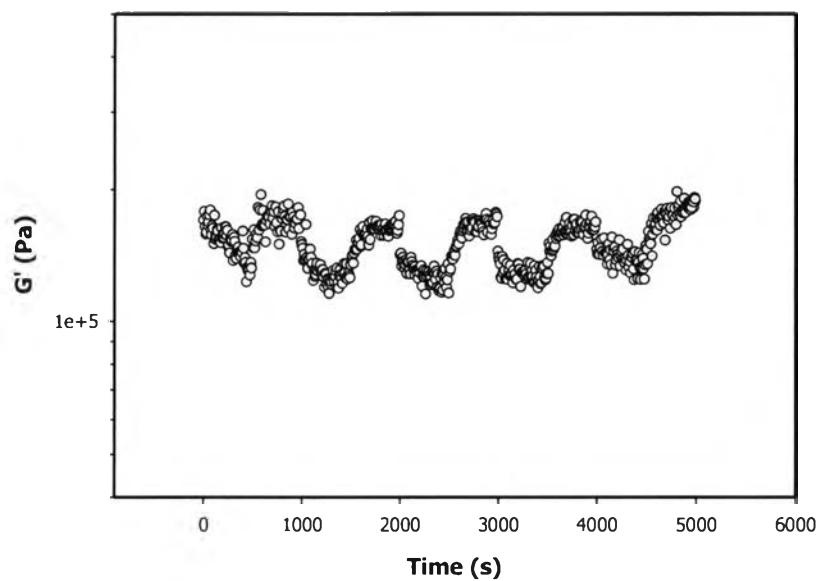
Figure K12 Temporal response of 0.05%v/v 30:1 dPPP/3%wt BPO cPCL(%strain 0.03, electric field strength of 2 kV, frequency 100 rad/s, film thickness 0.655 mm, 25°C).
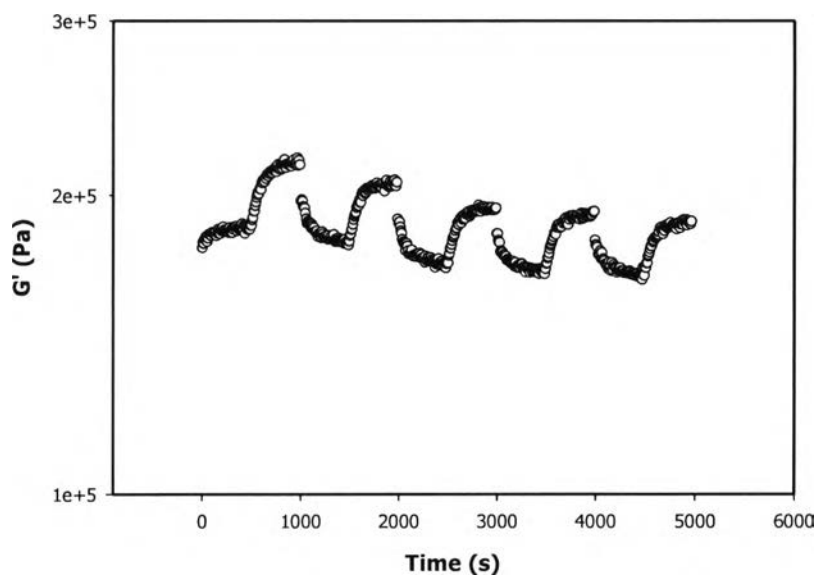
Figure K13 Temporal response of 0.1%v/v 30:1 dPPP/3%wt BPO cPCL(%strain 0.03, electric field strength of 2 kV, frequency 100 rad/s, film thickness 0.565 mm, 25°C).
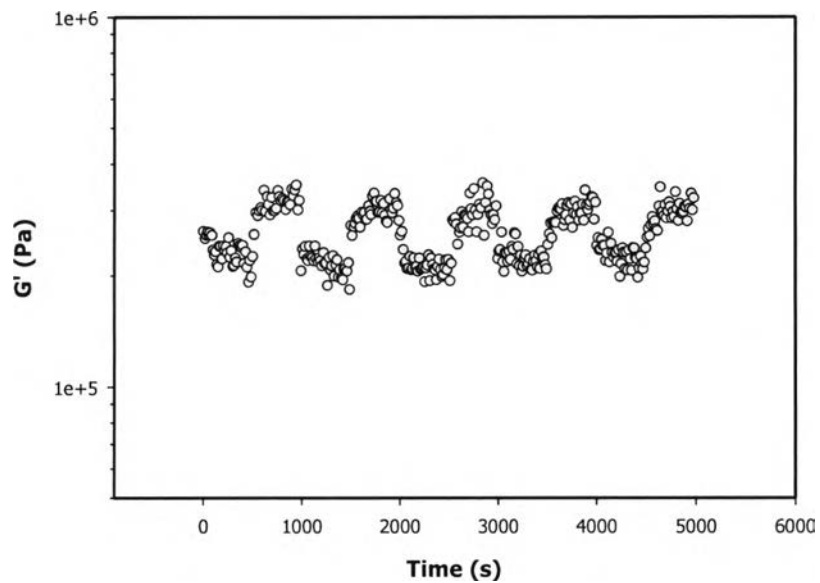
Figure K14 Temporal response of 0.5%v/v 30:1 dPPP/3%wt BPO cPCL(%strain 0.03, electric field strength of 2 kV, frequency 100 rad/s, film thickness 0.426 mm, 25°C).
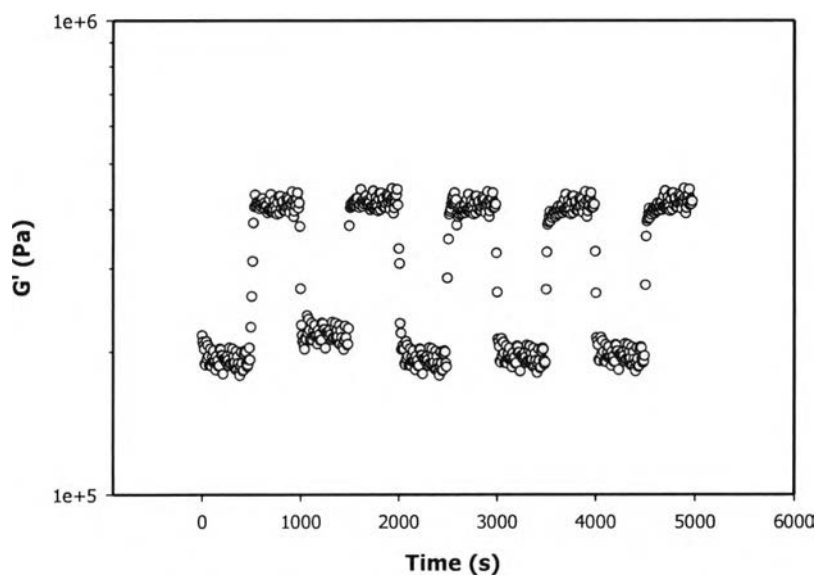
Figure K15 Temporal response of 1.0% v/v 30:1 dPPP/3%wt BPO cPCL(%strain 0.03, electric field strength of 2 kV, frequency 100 rad/s, film thickness 0.645 mm, 25°C).
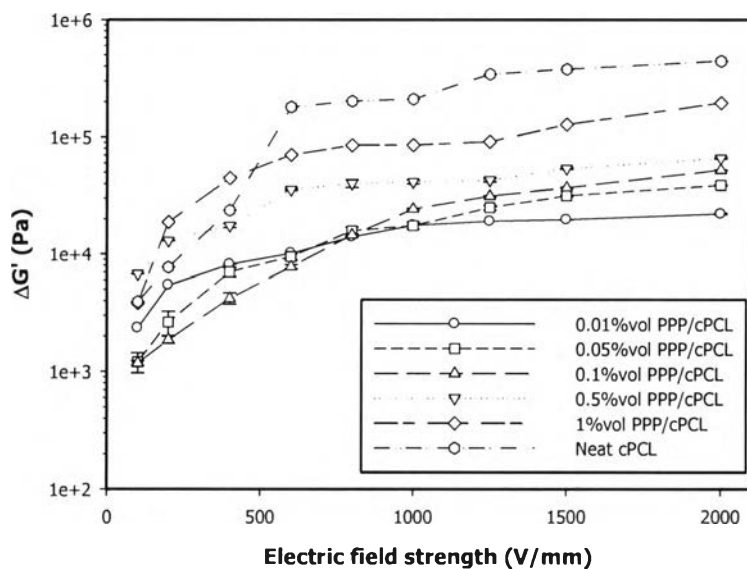
Figure J13 The comparison of storage modulus response ($\Delta G'$) as a function of electric field strength of neat cPCL and PPP/PCL composite at each concentration of embedded PPP.
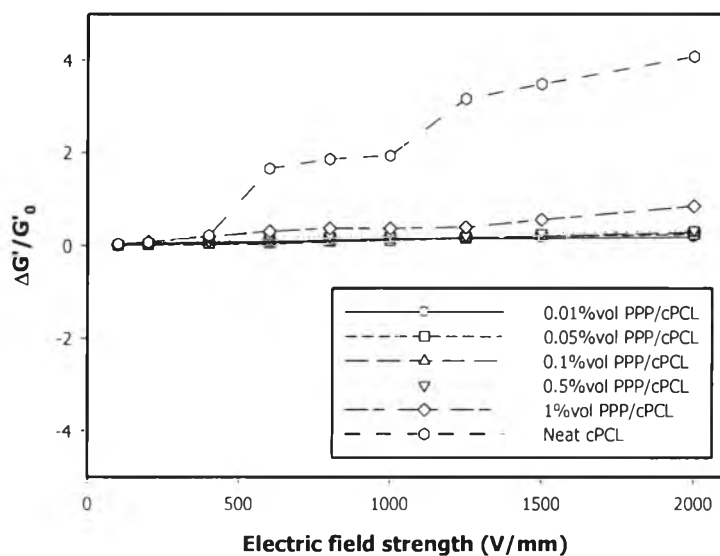
Figure K14 The comparison of storage modulus sensitivity($\Delta G'/G'_0$) as a function of electric field strength of neat cPCL and PPP/PCL composite at various concentration of embedded PPP.

Appendix L Dielectrophoretic Behavior

The dielectrophoresis forces of PCL, cPCL films and PPP/PCL composites were investigated by deflection experiment. A video camera was used to record the deflection. The induction time (τ_{ind}) and the recovery time (τ_{rec}) were observed. Next, pictures were captured from the video to measured The initial length (l_0), the deflection distances in x axis (d) and y axes (l') andthe deflection angle (θ) by using the SemAfore software (version 5.21). The electric field strength was varied between 0 and 500 V/mm at the room temperature. Then, the dielectrophoresis force (F_d) can be calculated from the static horizontal force balance consisting of the elastic force and the corrective gravity force term ($mgsin\theta$), as shown in this following equation:

$$F_d = F_e + mgsin\theta + \rho Vgsin\theta \text{ (N)} \qquad \text{(L1)}$$

All of the samples show that the more electric field strength applied, the more θ and F_d obtained. The 3%wt BPO cPCL has the highest deflection angle andielectrophoresis force because of the highest storage modulus sensitivity. In case of PPP/PCL composites, both $\theta$and F_d increase with increasing the composition of PPP in the system. which can be assigned to the increment of induced dipole moment in the sample.

Table L1 Dielectrophoretic Behavior of Neat PCL

Samples	E (V/mm)	θ	$F_x(\mu N)$	T_{ind} (s)	T_{rec} (s)
	0	0.00	0.00	0.00	0.00
	50	0.00	0.00	0.00	0.00
	100	0.14	1.12	0.00	0.00
	150	1.08	8.84	0.38	0.42
	200	1.33	10.96	0.47	0.49
	250	2.26	18.81	0.62	0.85
	300	2.59	21.56	0.67	1.39
	350	4.86	40.79	0.70	1.41
	400	6.28	53.13	0.82	1.47
	450	6.67	56.71	0.95	1.59
	500	6.94	59.50	1.07	1.82
	0	0.00	0.00	0.00	0.00
	50	0.00	0.00	0.00	0.00
	100	0.09	0.75	0.00	0.00
	150	1.14	8.99	0.34	0.47
	200	1.37	10.89	0.52	0.53
Neat PCL	250	2.33	18.77	0.66	0.92
	300	2.55	20.51	0.68	1.42
	350	4.82	39.12	0.74	1.45
	400	6.25	51.07	0.79	1.52
	450	6.56	53.88	0.93	1.67
	500	7.10	58.75	1.03	1.77
	0	0.00	0.00	0.00	0.00
	50	0.00	0.00	0.00	0.00
	100	0.16	1.16	0.00	0.00
	150	1.18	8.86	0.30	0.42
	200	1.32	10.01	0.54	0.57
	250	2.33	17.83	0.69	0.95
	300	2.51	19.14	0.70	1.41
	350	4.73	36.46	0.78	1.47
	400	6.33	49.19	0.83	1.60
	450	6.56	51.18	0.95	1.66
	500	7.10	55.81	1.12	1.84

Table L2 Dielectrophoretic Behavior of 3%wt BPO cPCL

Samples	E (V/mm)	θ	$F_d(\mu N)$	T_{ind} (s)	T_{rec} (s)
	0	0.00	0.00	0.00	0.00
	50	3.48	15.47	0.00	0.00
	100	4.38	19.50	0.45	1.48
	150	5.38	23.91	1.32	1.78
	200	8.14	41.31	1.74	2.54
	250	11.55	60.27	2.56	3.90
	300	20.49	107.62	3.89	4.26
	350	33.66	182.92	4.07	4.63
	400	45.56	265.29	4.52	5.34
	450	49.66	323.84	5.63	6.58
	500	58.72	444.38	6.08	7.10
	0	0.00	0.00	0.00	0.00
	50	2.96	13.01	0.00	0.00
	100	4.58	20.15	0.56	1.55
	150	5.38	23.64	1.43	1.87
	200	8.51	43.85	1.94	2.49
3% wt BPO cPCL	250	12.54	66.79	2.51	3.76
	300	20.57	110.74	3.73	4.37
	350	33.79	190.48	4.12	4.71
	400	46.04	283.24	4.74	5.47
	450	50.19	352.42	5.88	6.69
	500	58.93	490.69	6.20	7.07
	0	0.00	0.00	0.00	0.00
	50	3.04	13.52	0.00	0.00
	100	4.51	20.03	0.50	1.48
	150	6.19	27.50	1.42	1.79
	200	8.26	41.97	1.87	2.63
	250	11.23	58.62	2.48	3.92
	300	22.11	116.05	3.86	4.50
	350	34.22	186.13	4.34	4.83
	400	46.56	271.88	4.67	5.51
	450	50.19	328.74	5.77	6.70
	500	58.43	442.74	6.23	7.13

Table L3 Dielectrophoretic Behavior of 0.01% v/v 30:1 dPPP/3%wt BPO cPCL

Samples	E (V/mm)	θ	F_d(μN)	T_{ind} (s)	T_{rec} (s)
	0	0.00	0.00	0.00	0.00
	50	0.00	0.00	0.00	0.00
	100	0.00	0.00	0.00	0.00
	150	0.00	0.00	0.00	0.00
	200	2.60	17.12	0.42	1.21
	250	2.68	17.65	0.71	1.24
	300	3.04	20.01	1.5	1.51
	350	3.41	22.40	1.19	1.67
	400	4.71	30.92	1.32	1.97
	450	5.12	33.58	1.41	2.02
	500	5.16	33.92	1.76	2.21
	0	0.00	0.00	0.00	0.00
	50	0.00	0.00	0.00	0.00
	100	0.00	0.00	0.00	0.00
	150	0.00	0.00	0.00	0.00
0.01% v/v 30:1 dPPP/3%wt BPO cPCL	200	2.49	15.54	0.38	1.32
	250	2.75	17.19	0.73	1.36
	300	3.13	19.51	1.24	1.48
	350	3.33	20.77	1.25	1.67
	400	4.85	30.24	1.38	2.04
	450	5.49	34.17	1.57	2.07
	500	5.58	34.76	1.71	2.19
	0	0.00	0.00	0.00	0.00
	50	0.00	0.00	0.00	0.00
	100	0.00	0.00	0.00	0.00
	150	0.00	0.00	0.00	0.00
	200	2.61	16.79	0.41	1.22
	250	2.68	17.32	0.75	1.38
	300	2.92	18.80	1.17	1.41
	350	3.44	22.14	1.31	1.58
	400	4.72	30.32	1.38	2.00
	450	4.89	31.49	1.63	2.01
	500	5.31	34.13	1.78	2.14

Table L4 Dielectrophoretic Behavior of 0.05% v/v 30:1 dPPP/3%wt BPO cPCL

Samples	E (V/mm)	θ	$F_d(\mu N)$	T_{ind} (s)	T_{rec} (s)
	0	0.00	0.00	0.00	0.00
	50	0.00	0.00	0.00	0.00
	100	0.00	0.00	0.00	0.00
	150	0.00	0.00	0.00	0.00
	200	2.05	13.33	0.85	1.27
	250	2.68	17.51	1.02	1.69
	300	3.09	20.16	1.26	1.87
	350	3.78	24.66	1.58	2.01
	400	4.10	26.82	2.03	2.45
	450	4.82	31.42	2.14	2.51
	500	5.71	37.19	2.27	2.62
	0	0.00	0.00	0.00	0.00
	50	0.00	0.00	0.00	0.00
	100	0.00	0.00	0.00	0.00
	150	0.00	0.00	0.00	0.00
0.05% v/v 30:1 dPPP/3%wt BPO cPCL	200	2.08	13.08	0.78	1.34
	250	2.75	17.29	1.14	1.78
	300	3.13	19.67	1.30	1.88
	350	3.79	23.90	1.61	2.07
	400	4.05	25.54	2.12	2.52
	450	4.89	30.77	2.18	2.59
	500	5.61	35.31	2.25	2.74
	0	0.00	0.00	0.00	0.00
	50	0.00	0.00	0.00	0.00
	100	0.00	0.00	0.00	0.00
	150	0.00	0.00	0.00	0.00
	200	2.08	13.42	0.82	1.31
	250	2.75	17.73	1.12	1.67
	300	2.99	19.32	1.38	1.92
	350	3.84	24.81	1.74	2.10
	400	4.23	27.35	2.15	2.48
	450	4.93	31.85	2.25	2.52
	500	5.43	35.03	2.27	2.70

Table L5 Dielectrophoretic Behavior of 0.1% v/v 30:1 dPPP/3%wt BPO cPCL

Samples	E (V/mm)	θ	$F_d(\mu N)$	T_{ind} (s)	T_{rec} (s)
	0	0.00	0.00	0.00	0.00
	50	0.00	0.00	0.00	0.00
	100	0.00	0.00	0.77	1.03
	150	0.00	0.00	0.96	1.31
	200	2.96	20.39	1.07	1.39
	250	4.04	27.74	1.73	2.46
	300	8.53	58.20	1.88	2.49
	350	12.84	88.03	2.64	3.02
	400	14.81	101.20	2.80	3.24
	450	18.60	128.90	3.11	3.57
	500	23.68	164.18	3.87	4.83
	0	0.00	0.00	0.00	0.00
	50	0.00	0.00	0.00	0.00
	100	0.00	0.00	0.70	1.18
	150	0.00	0.00	0.90	1.26
0.1% v/v 30:1 dPPP/3%wt BPO cPCL	200	2.89	20.68	1.14	1.37
	250	3.86	27.49	1.23	2.54
	300	8.56	60.70	1.91	2.65
	350	12.88	91.704	2.53	3.11
	400	14.81	105.10	2.76	3.29
	450	18.82	135.49	3.02	3.72
	500	23.75	171.13	3.94	4.70
	0	0.00	0.00	0.00	0.00
	50	0.00	0.00	0.00	0.00
	100	0.00	0.00	0.63	1.14
	150	0.00	0.00	0.98	1.28
	200	2.75	19.10	1.18	1.31
	250	3.93	27.26	1.20	2.53
	300	8.79	60.59	1.97	2.57
	350	13.36	92.563	2.68	3.08
	400	14.70	101.50	2.77	3.34
	450	18.27	128.09	3.00	3.66
	500	24.07	168.77	4.02	4.98

Table L6 Dielectrophoretic Behavior of 0.5% v/v 30:1 dPPP/3%wt BPO cPCL

Samples	E (V/mm)	θ	$F_d(\mu N)$	T_{ind} (s)	T_{rec} (s)
	0	0.00	0.00	0.00	0.00
	50	0.00	0.00	0.00	0.00
	100	0.63	2.96	0.72	1.22
	150	2.04	11.67	0.99	1.58
	200	4.38	25.10	1.27	1.95
	250	6.83	39.22	1.88	2.73
	300	11.15	64.01	2.42	2.96
	350	15.57	89.52	2.66	3.10
	400	19.29	112.50	2.89	3.27
	450	24.84	146.31	3.41	3.98
	500	28.48	165.97	4.97	5.30
	0	0.00	0.00	0.00	0.00
	50	0.00	0.00	0.00	0.00
	100	0.82	4.39	0.66	1.13
	150	2.28	14.81	1.03	1.63
0.5% v/v	200	4.50	29.28	1.42	2.06
30:1	250	7.19	46.88	2.01	2.68
dPPP/3%wt	300	11.70	76.32	2.56	3.07
BPO cPCL	350	15.53	101.44	2.74	3.16
	400	18.40	122.07	2.90	3.34
	450	24.43	163.62	3.44	3.86
	500	28.73	190.30	4.72	5.42
	0	0.00	0.00	0.00	0.00
	50	0.00	0.00	0.00	0.00
	100	0.55	2.59	0.66	1.13
	150	2.52	15.03	1.03	1.63
	200	4.10	24.50	1.42	2.06
	250	7.03	42.13	2.01	2.68
	300	11.30	67.814	2.56	3.07
	350	15.57	93.64	2.74	3.16
	400	19.40	118.81	2.90	3.34
	450	24.84	154.21	3.44	3.86
	500	27.79	170.69	4.72	5.42

Table L7 Dielectrophoretic Behavior of 1.0% v/v 30:1 dPPP/3%wt BPO cPCL

| Samples	E (V/mm)	θ	$F_d(\mu N)$	T_{ind} (s)	T_{rec} (s)
	0	0.00	0.00	0.00	0.00
	50	0.00	0.00	0.00	0.00
	100	0.82	4.16	0.78	1.29
	150	4.13	27.15	1.77	2.52
	200	6.02	39.74	2.85	3.17
	250	9.97	65.67	3.21	3.98
	300	14.34	94.62	3.79	4.05
	350	19.97	132.20	4.22	4.61
	400	27.66	181.52	4.83	5.21
	450	30.86	206.28	5.33	5.51
	500	31.40	216.46	5.89	6.28
	0	0.00	0.00	0.00	0.00
	50	0.00	0.00	0.00	0.00
	100	1.09	5.78	0.96	1.33
	150	4.23	28.74	1.77	2.72
1.0% v/v	200	6.10	41.63	2.74	3.12
30:1	250	10.74	73.03	3.33	3.87
dPPP/3%wt	300	14.11	96.11	3.86	4.12
BPO cPCL	350	20.23	138.26	4.10	4.72
	400	27.67	187.42	4.73	5.30
	450	30.49	210.27	5.18	5.48
	500	31.61	224.76	6.04	6.37
	0	0.00	0.00	0.00	0.00
	50	0.00	0.00	0.00	0.00
	100	0.66	3.38	0.84	1.28
	150	4.07	27.55	1.64	2.83
	200	5.99	40.68	2.87	3.25
	250	9.78	66.28	3.15	3.88
	300	14.95	101.56	4.03	4.20
	350	19.38	132.35	4.18	4.70
	400	27.34	185.21	4.67	5.22
	450	30.89	213.60	5.25	5.54
	500	31.54	225.64	6.11	6.41
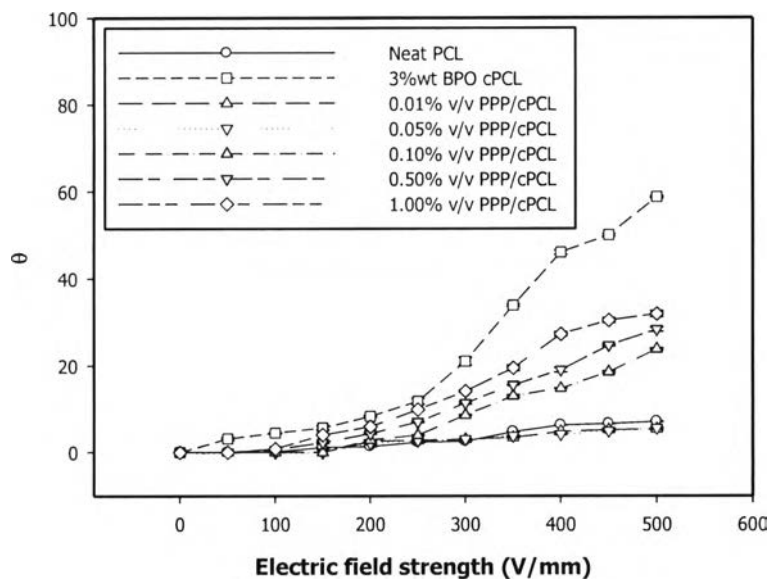
Figure L1 The comparison of deflection angle (θ) as a function of electric field strength of PCL films and PPP/PCL composites.
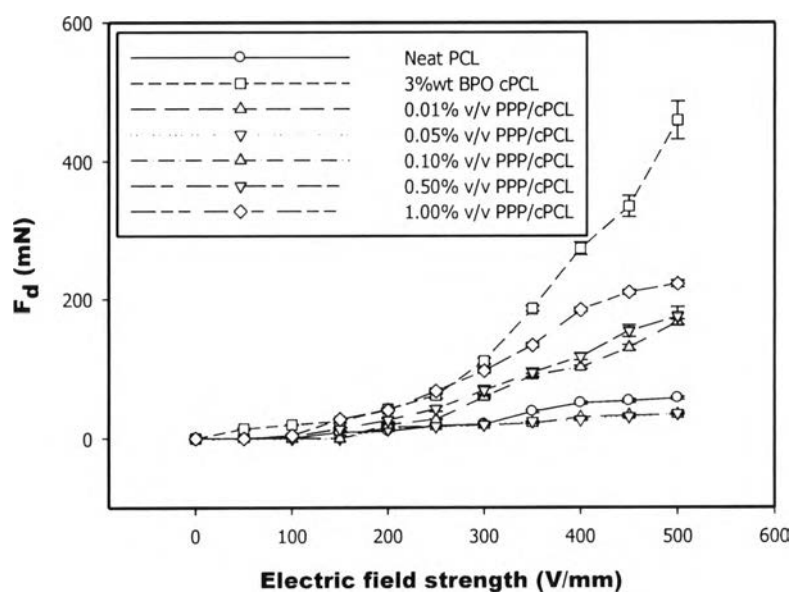
Figure L2 The comparison of dielectrophoresis force (F_d) as a function of electric field strength of PCL films and PPP/PCL composites.

(a)

(b)

(c)

(d)
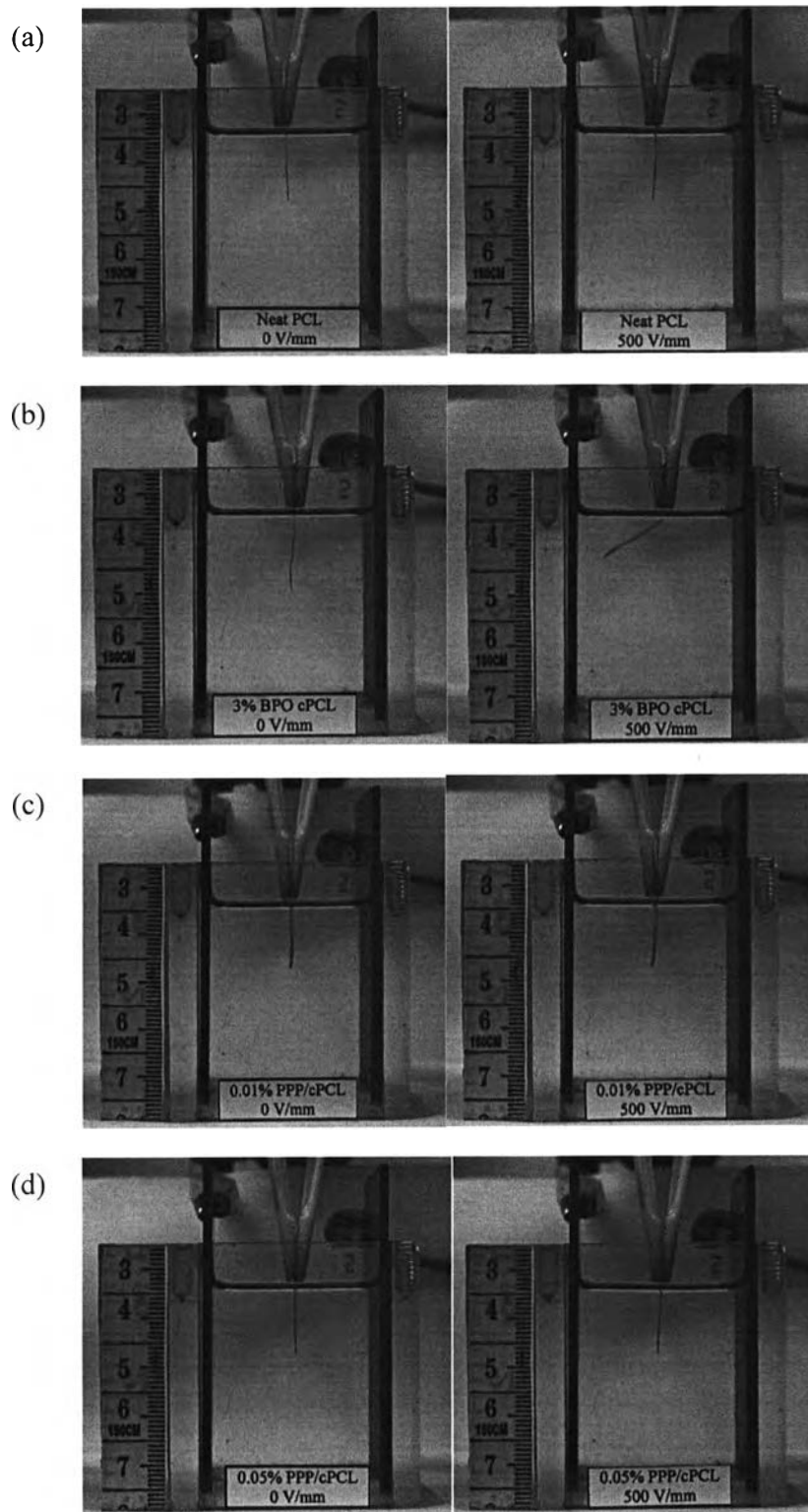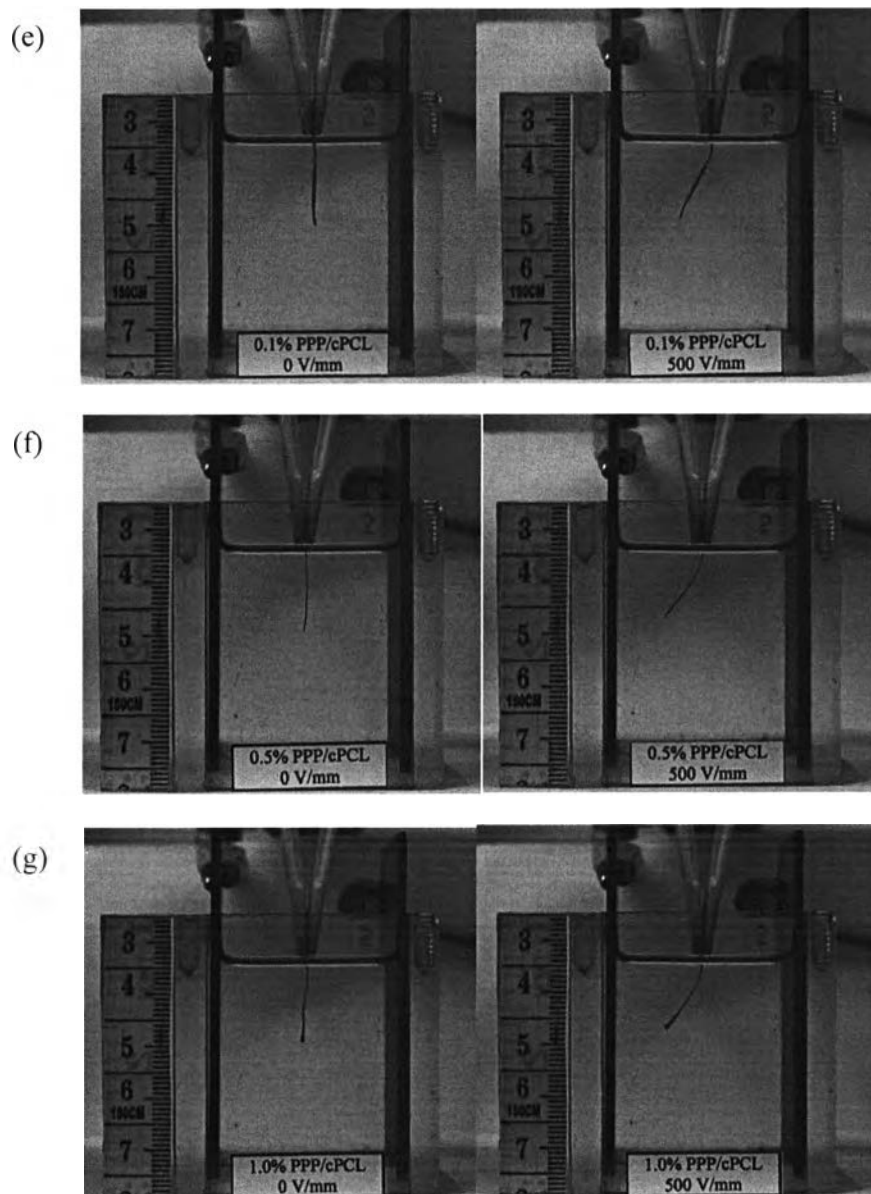
Figure L3 The deflection of a) Neat PCL b) 3%wt BPO cPCL c) 0.01% v/v 30:1 dPPP/3%wt BPO cPCL d) 0.05% v/v 30:1 dPPP/3%wt BPO cPCL e) 0.1% v/v 30:1 dPPP/3%wt BPO cPCL f) 0.5% v/v 30:1 dPPP/3%wt BPO cPCL and g)1.0% v/v 30:1 dPPP/3%wt BPO cPCL in the absence of electric field and under 500 V/mm of electric field.

Appendix M Mechanical Properties of PCL Films

Universal testing machine (Lloyd, LRX) was deployed to determined Young's modulus (E) of PCL films. First, the sample was cut into the rectangular shape (1x7x0.5 cm). The measurement was accomplished with the crosshead speed of 30 mm/min and the gauge length of 30 mm, which were adapted from ASTM 882. The result shows that Young's modulus decreases with increasing benzoyl peroxide (BPO) concentration, which were used as the crosslinking agent of PCL, corresponds with the restriction of the strain-induced crystallization that causes the strain hardening of the film. The higherBPO concentration, the more restriction of the induced crystallization is.
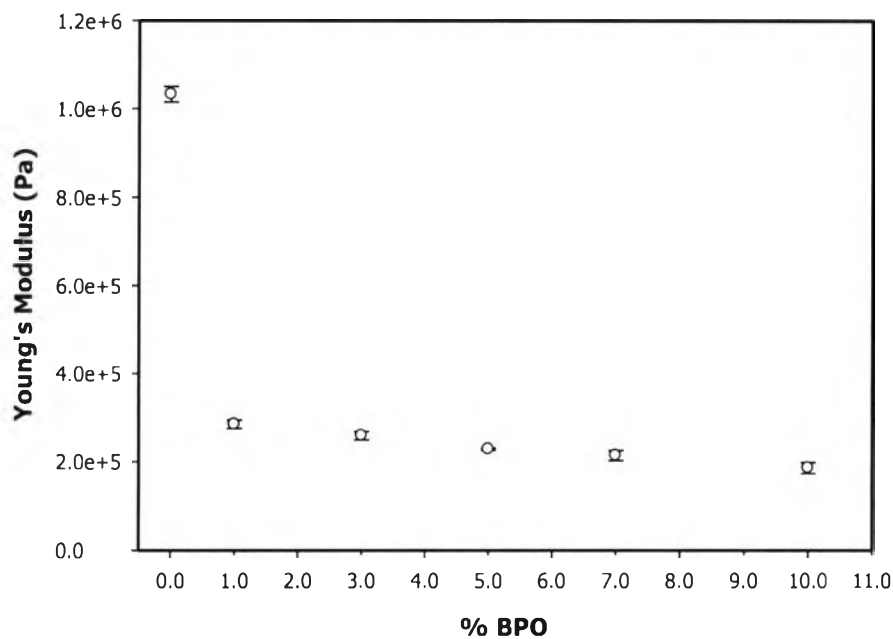
Figure M1 Young's modulus of the PCL films at various BPO concentration of.

Table M1 The raw data of Young's modulus of the PCL films at various concentration of BPO

Samples	Young's Modulus (kPa)	Standard Deviation (kPa)
Neat PCL	1,035.9	20.4
1 % wt BPO cPCL	284.6	9.4
3 % wt BPO cPCL	259.2	9.7
5 % wt BPO cPCL	228.9	2.7
7 % wt BPO cPCL	213.9	11.3
10 % wt BPO cPCL	185.8	12.3

Table M2 Young's modulus compared to previous works

% wt of BPO	E (MPa)	E (MPa) Mo-ling *et al.*, 1999	E (MPa) Han et al., 2007
0	1,032.6	362.3	284
1.0	284.6	317.8	257
3.0	259.2	193.3	230
5.0	228.9	194.8	-
10.0	185.8	117.8	-

CURRICULUM VITAE

Name: Mr. Napat Charoonrak

Date of Birth: April 11, 1989

Nationality: Thai

University Education:

2007–2010 Bachelor Degree of Materials Science, Faculty of Sciences, Chulalongkorn University, Bangkok, Thailand

Proceedings:

1. Charoonrak, N.; and Sirivat, A. (2013, April 23) Development of Poly(p-phenylene)/Crosslinked Poly(ε-caprolactone) as Electroactive Shape Memory Composite. Proceedings of The 4th Research Symposium on Petrochemical and Materials Technology and the 19th PPC Symposium on Petroleum, Petrochemicals, and Polymers, Bangkok, Thailand.

Presentations:

1. Charoonrak, N.; and Sirivat, A. (2013, April 22) Development of Poly(ε-caprolactone)/Poly(p-phenylene) as Electroactive Shape Memory Polymer Blend. Paper presented at The 1st Annual Symposium of Conductive and Electroactive, Bangkok, Thailand.

2. Charoonrak, N.; and Sirivat, A. (2013, April 23) Development of Poly(p-phenylene)/Crosslinked Poly(ε-caprolactone) as Electroactive Shape Memory Composite. Paper presented at The 4th Research Symposium on Petrochemical and Materials Technology and the 19th PPC Symposium on Petroleum, Petrochemicals, and Polymers, Bangkok, Thailand.

3. Charoonrak, N.; and Sirivat, A. (2013, May 21-23) Development of Poly(para-phenylene)/ Poly(ε-caprolactone) as Electroactive Shape Memory Composite. Paper presented at The 3rd International Symposium Frontiers in Polymer Science in Association with the Journal Polymer, Sitges, Spain.